

# ON THE BARYONIC, STELLAR, AND LUMINOUS SCALING RELATIONS OF DISK GALAXIES

V. AVILA-REESE<sup>1</sup>, J. ZAVALA<sup>2,3</sup>, C. FIRMANI<sup>4,1</sup>, AND H. M. HERNÁNDEZ-TOLEDO<sup>1</sup>

*To appear in Astronomical Journal*

## ABSTRACT

We explore how the slopes and scatters of the scaling relations of disk galaxies ( $V_m$ - $L$ [- $M$ ],  $R$ - $L$ [- $M$ ], and  $V_m$ - $R$ ) do change when moving from  $B$  to  $K$  bands and to stellar and baryonic quantities. For our compiled sample of 76 normal, non-interacting high and low surface brightness (SB) disk galaxies, we find important changes, which evidence evolution effects, mainly related to the gas infall and star formation (SF) processes. We also explore correlations among the  $(B - K)$  color, stellar mass fraction  $f_s$ , mass  $M$  (luminosity  $L$ ), and surface density (SB), as well as correlations among the residuals of the scaling relations, and among these residuals and those of the other relations studied here. Some of our findings are: (i) the scale length  $R_{\text{bar}}$  is a third parameter in the baryonic Tully–Fisher relation (TFR) and the residuals of this relation follow a trend (slope  $\approx -0.15$ ) with the residuals of the  $R_{\text{bar}}$ - $M_{\text{bar}}$  relation; for the stellar and  $K$  band cases, the scale length is not anymore a third parameter and the mentioned trend disappears; (ii) among the TFRs, the  $B$ -band TFR is the most scattered; in this case, the color is a third parameter, in agreement with previous works; (iii) the low SB galaxies break some observed trends in diagrams that include surface density, color, and  $f_s$ , suggesting then a threshold in the gas surface density  $\Sigma_g$ , below which the SF becomes independent of the gas infall rate and  $\Sigma_g$ . Our results are interpreted and discussed in the light of  $\Lambda$ CDM-based models of disk galaxy formation and evolution. These models are able to explain not only the baryonic scaling correlations, but also most of the processes responsible for the observed changes in the slopes, scatters, and correlations among the residuals when changing to stellar and luminous quantities. The galaxy baryon fraction,  $f_{\text{gal}}$ , is required to be smaller than 0.05 on average. We detect some potential difficulties for the models: the observed color- $M$  and surface density- $M$  correlations are steeper, and the intrinsic scatter in the baryonic TFR is smaller than those predicted.

*Subject headings:* Cosmology: dark matter Galaxies: evolution – Galaxies: fundamental parameters – Galaxies: spiral – Galaxies: structure

## 1. INTRODUCTION

Disk galaxies are the main population of galaxies in the local Universe. The study of their global scaling relations is of paramount relevance for understanding the formation and evolution of galaxies in general. The main disk galaxy observed global scaling relations are those between maximum circular velocity,  $V_m$ , and luminosity,  $L$ ; between disk scale length,  $R$ , and  $L$ ; and between  $V_m$  and  $R$ . Each one of these relations can be established for different optical/NIR pass-bands. Under some assumptions, analogous relations can be calculated for the corresponding stellar and baryonic quantities. The changes in the zero points, slopes and scatters of these relations, when changing from one color band to another, and to stellar and baryonic quantities, are expected to be intimately related to the stellar population properties and radial distributions of disk galaxies. In its turn, these properties and distributions depend mainly on the disk assembly and star formation (hereafter SF) histories. Therefore, the study of the scale relations for different pass-bands and for the stellar and baryonic cases offers valuable information on the structural, dynamical

and SF properties of disk galaxies, as well as important constraints on models of their formation and evolution. The present paper is focused on this study.

### 1.1. Background on the disk scaling relations

The most robust and studied of the disk galaxy scaling relations is the one between  $L$  and  $V_m$ , the so-called Tully–Fisher relation (TFR). Originally discovered in the  $B$  pass-band (Tully & Fisher 1977), it was afterward shown that it also applies to infrared bands. More recently, after applying a velocity (luminosity)–dependent extinction correction, Tully & Pierce (2000) have confirmed that the slope of the  $L$ - $V_m$  correlation gets steeper systematically from  $B$  ( $\approx 2.9$ ) to  $K$  ( $\approx 3.5$ ) bands. This result suggests some dependence of galaxy colors on  $V_m$  for a given galaxy luminosity or mass. The amplitude of the scatter of the TFRs changes also with wavelength. These dependencies of the slope and scatter of the TFR on wavelength are related mainly to stellar population effects, which on their own, are related to the assembly and SF histories of galaxies. Regarding the intrinsic TFR scatters, they are found to be small, posing a challenge for scenarios aimed to explain the origin of disk galaxies (Eisenstein & Loeb 1996; Avila-Reese et al. 1998; Mo et al. 1998; Firmani & Avila-Reese 2000).

The TFR has been widely studied for estimating extragalactic distances. In this case the independent variable (predictor) is the circular velocity, and the galaxy samples are carefully pruned to minimize the scatter. The latter implies a selection of samples for a narrow range of

<sup>1</sup> Instituto de Astronomía, Universidad Nacional Autónoma de México, A.P. 70-264, 04510 México D. F., México

<sup>2</sup> Instituto de Ciencias Nucleares, Universidad Nacional Autónoma de México, A.P. 70-543, 04510 México D.F., México.

<sup>3</sup> *Present affiliation:* Shanghai Astronomical Observatory, Nandan Road 80, Shanghai 200030, China; jzavala@shao.ac.cn

<sup>4</sup> INAF-Osservatorio Astronomico di Brera, via E.Bianchi 46, I-23807 Merate, Italy

morphological types and surface brightnesses (hereafter SBs). However, for studies aimed to understand the origin of the TFR and use it to constrain models of galaxy formation rather than circular velocity, the luminosity should be the predictor, and the sample should be as wide as possible in morphological types, SBs, and colors (Courteau et al. 2007). Hereafter, we will refer to the TFR as the  $V_m$ - $L$ (- $M$ ) correlation.

By using NIR magnitudes –which are good tracers of stellar masses– and gas contents when available, some authors calculated the stellar and baryonic TFRs (e.g., McGaugh et al. 2000; Bell & de Jong 2001; Meyer & Moore 2004; Gurovich et al. 2004; Pizagno et al. 2005; de Rijcke et al. 2007). As discussed in Firmani & Avila-Reese (2000; hereafter FA-R), on one hand the baryonic TFR appears to be closely related to the cosmological halo maximum circular velocity–mass relation, and on the other hand, when compared to the stellar TFR, it reflects some aspects of the SF efficiency for different types of galaxies. The behavior of the scatter, when one changes from  $B$ – to  $K$ –band TFRs and to the stellar and baryonic TFRs, certainly contains relevant information on the processes of disk galaxy evolution such as gas infall, SF, and stellar population histories.

The radius for a given luminosity (or the disk SB) has been considered as a potential third parameter that correlates with the scatter of the TFR (e.g., Kodaira 1989; Willick 1999). The scale length  $R$  is indeed another structural parameter of disk galaxies that spans a wide range of values. Some authors have reported that the scatter of the TFR is reduced up to 50% when introducing  $R$  as a third parameter (e.g., Koda, Sofue & Wada 2000; Han et al. 2001). However, if the scatter of a given relation decreases by introducing a third variable, it does not necessary mean that such a variable is a statistically significant parameter. Indeed, some authors have shown that  $R$  (or central SB) is not a physical third parameter in the TFR (e.g., Han 1991; Tully & Verheijen 1997; Willick et al. 1997; Courteau & Rix 1999; FA-R), but radius could be a third parameter in the baryonic TFR (FA-R; Avila-Reese, Firmani & Zavala 2002; Zavala 2003; Dutton et al. 2007).

It is well known that radius does correlate with  $L$  (Freeman 1970) and  $V_m$  (Tully & Fisher 1977), although these correlations are much more scattered than the TFR. Disk galaxies in the  $\text{Log}L$ – $\text{Log}V_m$ – $\text{Log}R$  parameter space indeed lie in a thin oblique plane whose edge-on projection is close to the  $\text{Log}L$ – $\text{Log}V_m$  (TFR) projection (Koda, Sofue & Wada 2000; Han et al. 2001; Shen, Mo & Shu 2001; Gnedin et al. 2007). This is the so called fundamental plane of disk galaxies. Here we construct from observations and analyze separately each one of the three projections of these planes.

### 1.2. Construction and interpretation of the scaling relations: how do they change from luminous to stellar and baryonic quantities?

In most of the previous works, the disk galaxy scaling correlations were constructed for samples biased in morphological types and SBs (pruned for reducing the scatter), and without selecting the environment. However, *for theoretical and interpretative studies, the observational galaxy sample should be as wide as possible in the range of morphologies, SBs, and colors* in order to

include the whole population of disk galaxies, later to be compared with model predictions. Besides, since galaxy models are commonly for isolated galaxies, the observational sample should also be selected to contain galaxies *not affected by the environment*. On the other hand, the limited information of the samples employed in previous works, did not allow to explore how the scaling correlations and their scatters change from luminous to stellar and baryonic quantities.

In this paper we shall use a sample of 76 disk galaxies compiled from the literature and homogenized in Zavala et al. (2003a; hereafter ZAHF) and Zavala (2003). This sample is not in any sense complete, an aspect that is crucial for volume-averaged population studies (e.g., the luminosity function), but it is less relevant for studies on the correlations of physical properties. The sample includes high and low SB (hereafter HSB and LSB, respectively) disk *normal*<sup>5</sup> galaxies of all morphological types, and it provides photometric information, at least in  $B$  and  $K$  bands, as well as information on the rotation curve and the HI integrated flux. None of the previous related works have presented a sample with these characteristics, which are crucial for the analysis proposed here. By using this sample, we will explore the differences in the slope and scatter of each scaling relation defined in the  $B$  and  $K$  bands, and for stellar and baryonic quantities. The results of this exploration will be interpreted in the light of disk galaxy formation and evolution models.

The current theory of galaxy formation and evolution is based on the hierarchical  $\Lambda$  Cold Dark Matter ( $\Lambda$ CDM) cosmological model (see for recent reviews Avila-Reese 2006; Baugh 2006). Several authors have attempted to predict the scaling relations of disk galaxies and their scatters within this model (e.g., Avila-Reese et al. 1998, 2002; Mo et al. 1998; Navarro & Steinmetz 1999, 2000; FA-R; Koda et al. 2000; Shen et al. 2001; Zavala 2003; Courteau et al. 2003, 2007; Dutton et al. 2005, 2007; Gnedin et al. 2007; Courteau et al. 2007). The results are encouraging. We shall use some of these results, mainly those of FA-R, to interpret and discuss the new inferences from observations presented here.

Notice that it was a common practice in the literature to compare model results with the observed *luminous* properties and correlations, while most of the galaxy models did not actually include or treat self-consistently the process of gas transformation into stars, as well as did not follow the evolutionary path of halos and galaxies. As FA-R showed (see also Avila-Reese et al. 2002; Dutton et al. 2005), on one hand, there are systematical differences in the predicted scaling relations and their scatters among the luminous, stellar, and baryonic quantities; differences that we will explore here. On the other hand, properties like the stellar and baryonic  $M$ ,  $R$ ,  $V_m$ , gas fraction, and integral colors depend not only on the initial parameters, but also on the evolutionary path of the halo–disk system (Stringer & Benson 2008). Contrary to the “static population” models, like those of Mo et al. (1998) and extensions of them, the FA-R models are evolutionary. Under some simplifications, they follow self-consistently (see Appendix B): the halo and disk assembly, taking into account the halo adiabatic

<sup>5</sup> Here we understand by normal galaxies: non-dwarf, non-interacting, nearly isolated local galaxies.

contraction; the self-regulated disk SF and feedback; the luminosity evolution; and the secular bulge formation.

During the completion of the present work, several of the mentioned papers above, with results and with a philosophy similar to ours, appeared in the literature. Although some overlapping is present, our contribution is original in the sense that we focus the research *on the changes in the scaling relations and their scatters when moving from optical to NIR bands and to stellar and baryonic quantities*. Our sample is similar in number to others used in recent works (e.g., Gnedin et al. 2007) and smaller with respect to Dutton et al. (2007) and Courteau et al. (2007), who use  $\sim 1300$  objects with  $I$ -band photometry and  $H\alpha$  cinematics, but only  $\sim 360$  out of them, mainly HSB galaxies, have available  $K$ -band photometry. These large samples are undoubtedly useful and we will compare, when possible, with their results. However, we can not use them because they lack several observables (e.g., gas content, optical photometry) and requirements (e.g., inclination limits, LSB galaxies in both optical and  $K$  bands) that we have imposed for our study. We hope that our study will serve as a benchmark for similar analyzes based on large multiwavelength galaxy surveys, which are currently being completed.

The paper is organized as follows. In §2 we describe the disk galaxy sample to be used. The three main scaling correlations and their scatters are constructed and discussed in §3 for bands  $B$  and  $K$  and for the inferred stellar and baryonic quantities. Some other correlations among global galaxy quantities are also reported. In §4, in the light of previous  $\Lambda$ CDM-based disk galaxy formation and evolution models, we interpret the changes in the slopes and scatters of the scaling relations when changing from  $B$  to  $K$  bands and to stellar and baryonic quantities. A summary of the results and the conclusions of this work are presented in §5.

## 2. THE SAMPLE

In the literature there are only a few small galaxy samples with the requirements and data we need (broad in morphological types and SBs, with information on detailed surface-photometry in two separated pass-bands, e.g.  $B$  and  $K$ , on global dynamics, and on total HI gas flux). Here we use a compilation and completion of these samples presented in ZAHF and Zavala (2003; see also Graham 2002). In the following, we present the sub-samples, describe the homogenization and data correction processes that we have implemented, and the way in which we calculated the stellar and baryonic quantities (see ZAHF for additional details).

The sub-samples are: (i) de Jong & van der Kruit (1994; see also de Jong 1996a), which comprises undisturbed field, mostly HSB, disk galaxies, (ii) Verheijen (1997; see also Verheijen & Sancisi 2001), composed of disk HSB and LSB galaxies from the least massive and most spiral-rich nearby cluster, Ursa Minor, and (iii) Bell et al. (2000), a sample of LSB galaxies observed partially by them; the rest were compiled from the literature, mainly from de Blok, van der Hulst & Bothun (1995), and de Blok, McGaugh & van der Hulst (1996). We also included in our sample the Milky Way and Andromeda galaxies.

The raw photometric magnitudes, disk scale lengths,  $R$ , and central SBs were taken directly from the source

papers. In ZAHF and Zavala (2003) we have checked that there were no significant systematic differences in these parameters with inclination; we found also no systematics due to the different completeness criteria and profile fitting procedures used by the original authors of each sub-sample. In fact, the dominant source of error in the photometric parameters is caused by the uncertainty in the sky level (Bell et al 2000; de Jong 1996a). Regarding the dynamical information, and to make the data as uniform as possible, we used the velocity line-width  $W_{20}$  (defined at the 20% level) for almost all the galaxies in the sample. Only a few (LSB) galaxies in the sample lack a  $W_{20}$  measurement but have measured rotation curves; in these cases we have used the  $V_m$  inferred directly from the rotation curve. If properly corrected,  $W_{20} \approx 2V_m$  (Verheijen 1997; Verheijen & Sancisi 2001). For the Verheijen sub-sample, we adopt the  $W_{20}$  values given in Verheijen & Sancisi (2001), while for the de Jong sub-sample and most of the LSB galaxies from the Bell et al. sub-sample,  $W_{20}$  was extracted from the HyperLEDA information system<sup>6</sup>. The integral fluxes in the 21-cm line (used to calculate the neutral gas mass component in galaxies) were taken from HyperLEDA, Verheijen & Sancisi (2001), and de Blok et al. (1996).

A condition imposed on our sample is that galaxies should be in a restricted range of inclinations ( $35^\circ \leq i \leq 80^\circ$ ). We excluded from the sample galaxies with clear signs of interaction (mainly from the Verheijen sub-sample) and with rotation curves that are still increasing at the last measured outer radius. Only some LSB galaxies showed this feature. The final sample consists of 76 galaxies: 42 out of 86, 29 out of 52, and 5 (8) out of 23 from the de Jong, Verheijen, and Bell et al. sub-samples, respectively, plus the Milky Way and Andromeda galaxies. From the Bell et al. (2000) sample, 8 LSB galaxies are useful for us, but three of them are in common with the de Jong sample.

The local distances to the galaxies were calculated using the kinematic distance modulus given in HyperLEDA (see more details in ZAHF). The value of the Hubble constant used in this database is the same we assume here,  $H_0 = 70 \text{ km s}^{-1} \text{ Mpc}^{-1}$ . Since the LSB galaxies from the Bell et al. sub-sample are not included in HyperLEDA, their distances were taken directly from the source paper, properly corrected for the  $H_0$  value used here.

The compiled sample is not complete in any sense, but it comprises representative ranges of the basic features of *normal* disk galaxies (see Fig. 1 in ZAHF). These features are mainly the morphological type, magnitude, disk central SB, integral color, and gas fraction.

### 2.1. Data corrections

The total magnitudes were corrected for Galactic extinction (following Schlegel et al. 1998),  $K$  term, and internal extinction (see ZAHF for details). For the latter we used the empirical velocity- (luminosity-) dependent extinction coefficients determined by Tully et al. (1998). The central SBs were corrected for Galactic extinction,  $K$  term, cosmological SB dimming, and inclination-geometrical and extinction effects- (see ZAHF). For the inclination correction, we followed Verheijen (1997), considering LSB galaxies optically thin in all bands. The

<sup>6</sup> <http://leda.univ-lyon1.fr>

HSB galaxies were also considered optically thin in the  $K$  band. We have defined LSB galaxies as those with central SB's in the  $K$  band, after SB correction, larger than  $18.5 \text{ mag/arcsec}^2$  (Verheijen 1997). The 21 cm line-widths at the 20% level,  $W_{20}$ , for the Verheijen subsample were taken directly from Verheijen & Sancisi (2001). Galaxies with  $W_{20}$  taken from LEDA were de-corrected (for instrumental corrections) to get the raw data (Paturel et al. 1997), and then corrected again for broadening due to turbulent motions and for inclination, this time following the procedure by Verheijen & Sancisi (2001).

In ZAHF we did not take into account the observational errors. Here we attempt to estimate these errors for both the photometric and dynamic parameters, and use them for our results when possible. In the Appendix A, we present our approach to estimate the errors.

## 2.2. Composite quantities

The stellar mass and disk central surface density,  $M_s$  and  $\Sigma_{s,0}$ , were derived from the  $K$ -band luminosity (which includes the bulge) and the extrapolated disk central SB,  $\Sigma_{K,0}$ , respectively, by using the appropriate stellar mass-to-light ratio,  $\Upsilon_K$ . The application of population synthesis techniques to disk galaxy evolution models show that  $\Upsilon_K$  depends mainly on the integral color (Tinsley 1981; Bruzual 1983; Bell & de Jong 2001). In ZAHF we have used a  $\Upsilon_K$  inferred from the latter paper. In a more recent work, Bell et al. (2003) used galaxy evolution model fits for a large sample of galaxies from the Two Micron All Sky Survey and the Sloan Digital Sky Survey (SDSS). They obtained a correlation of  $\Upsilon_K$  with  $(B - R)$  color which is shallower and more scattered than in Bell & de Jong (2001). Unfortunately, Bell et al. (2003) did not report the correlation of  $\Upsilon_K$  with the  $(B - K)$  color. We have obtained this correlation by a re-scaling procedure that makes use of the  $\Upsilon_K$ -( $B - R$ ) correlation given in Bell et al. (2003), and the  $\Upsilon_K$ -( $B - R$ ) and  $\Upsilon_K$ -( $B - K$ ) correlations given in Bell & de Jong (2001; their model “formation epoch with bursts” was used). We obtain the following result:

$$\text{Log} \Upsilon_K = -0.38 + 0.08(B - K). \quad (1)$$

For low SB values, at least for blue galaxies,  $\Upsilon_K$  seems to anti-correlate with color (Verheijen 1997). In Fig. 1 of Bell & de Jong (2001), it is also shown how the inferred values of  $\Upsilon_K$ , for low SBs, do not decrease anymore with decreasing SB, and even start to increase as SB decreases, although the scatter is large. In the absence of detailed models, we approximate the  $\Upsilon_K$ -( $B - K$ ) correlation for LSB galaxies in such a way that for  $(B - K) > 3$ ,  $\Upsilon_K$  is given by eq. (1), while for  $(B - K) \leq 3$ ,

$$\Upsilon_K = 1.90 - 0.40(B - K). \quad (2)$$

The latter dependence is from a linear eye-fit to the  $\Upsilon_K$ -( $B - K$ ) correlation of the *blue* LSB galaxies in Verheijen (1997), for his case of an Hernquist halo model and the constrained decomposition method. After using the new  $\Upsilon_K$ -( $B - K$ ) correlations, the galaxy stellar and baryonic masses calculated here are slightly different from the ones used in ZAHF. The scale length of the stellar disk,  $R_s$ , is assumed to be equal to the scale length in the band  $K$ ,  $R_K$ . Most of the stars in the disk are properly traced using this band.

The disk gas mass,  $M_g$ , is estimated as:

$$M_g = 1.4 M_{\text{HI}} \left[ 1 + \frac{M_{\text{H}_2}}{M_{\text{HI}}} \right] \quad (3)$$

where the factor 1.4 takes into account helium and metals, and  $M_{\text{H}_2}$  is the mass in molecular hydrogen. The  $M_{\text{H}_2}/M_{\text{HI}}$  ratio has been found to depend on the morphological type  $T$  (Young & Knesek 1989). Using the latter paper, McGaugh & de Blok (1997) estimated that  $M_{\text{H}_2}/M_{\text{HI}} = 3.7 - 0.8T + 0.043T^2$ . For  $T < 2$ , this empirical fitting formula could overestimate the gas mass in galaxies, thus we assume:  $M_{\text{H}_2}/M_{\text{HI}} = 2.3$  (the value of the fit at  $T = 2$ ) for  $T < 2$ .

The galaxy baryonic mass is defined as  $M_{\text{bar}} = M_s + M_g$ , and the gas mass fraction as  $f_g = M_g/M_{\text{bar}}$ . Unfortunately, we do not have information on the gas surface density profile parameters ( $\Sigma_{g,0}$  and  $h_g$ ) for the galaxies in our sample. We need them in order to calculate the baryonic disk central surface densities,  $\Sigma_{\text{bar},0}$ , and scale lengths,  $R_{\text{bar}}$ . As discussed in ZAHF, we assume that the total gas surface density follows an exponential distribution with an scale length 3 times that of  $R_K$ . Thus,  $\Sigma_{g,0} = M_g/2\pi(3R_K)^2$ . The baryonic quantity  $\Sigma_{\text{bar},0}$  is then calculated as  $\Sigma_{\text{bar},0} = \Sigma_{s,0} + \Sigma_{g,0}$ . The corresponding baryonic radius will be then  $R_{\text{bar}} = R_K[(\Sigma_{s,0} + 9\Sigma_{g,0})/\Sigma_{\text{bar},0}]^{0.5}$ . In fact, the addition of the (uncertain) gas disk parameters will have little impact on our final results. This inclusion is important only for gas rich galaxies (late-type, blue LSB galaxies). We believe that in spite of the uncertainties, some real systematical variations of the baryonic disk scale length and surface density with the gas content of galaxies can still be taken into account through our procedure.

We have also estimated the errors in the composite quantities by adequately propagating the errors of the primary quantities. See Appendix A for details.

## 3. THE SCALING RELATIONS AND THEIR DISPERSIONS

For the sample of 76 galaxies presented in §2, we proceed to construct the physical scaling relations  $V_m$ - $L$  ( $-M$ ),  $R$ - $L$  ( $-M$ ), and  $V_m$ - $R$  in the bands  $B$  and  $K$ , and for stars and baryons. Some authors recommend to use  $V_{\text{flat}}$ , the outer asymptotic flat part of the rotation curve, as an estimate of the circular velocity, instead of  $V_m$ . We stress that for studies aiming to understand the origin of the TFR and its scatter (the same applies for the  $V_m$ - $R$  relation) as well as to compare them with galaxy model predictions, the adequate quantity to be used is  $V_m$  *because it maximizes the contribution of the disk component for a given halo*. By using  $V_{\text{flat}}$ , which traces the dynamics of the galaxy in outer regions, where the halo component tends to dominate, we loose information about the disk contribution. In fact, here we do not use neither  $V_m$  nor  $V_{\text{flat}}$ , but  $W_{20}$ . However, as mentioned in §2, there is some evidence that  $W_{20} \approx 2V_m$ .

For the luminosities and masses, here we use the total ones, i.e. the sum of disk and bulge. For the cases when bulges form by disk secular evolution processes (e.g. Avila-Reese & Firmani 2000; Avila-Reese et al. 2005), this is a good approximation for total disk luminosities and masses. For the scale length, the corresponding  $B$  and  $K$  band radii are used in the luminous scaling relations. For the stellar and baryonic scaling relations

we assume respectively  $R_s=R_K$  and a scale length,  $R_{\text{bar}}$ , which takes into account the sum of the stellar and gas disks (see §2.2).

In Figs. 1, 2, and 3, the observational points with the estimated error bars are plotted in the diagrams corresponding to the disk galaxy scaling relations studied here. The variables are given logarithmically. Circles and triangles are for galaxies with  $(B - K) > 3.0$  (red) and  $\leq 3.0$  (blue), respectively. Open and solid symbols are for galaxies with  $\mu_{K,0} \leq 18.5$  (HSB) and  $\mu_{K,0} > 18.5$  (LSB), respectively. To quantify the correlations and compare them among the different pass-bands and mass quantities (and eventually to model predictions), one needs to fit the correlations. To this end, a linear regression analysis should be used. We recall that our aim here is to explore variations for the scaling relations in the different cases ( $B$  and  $K$  bands, stars, and baryons) rather than study in detail the relations for each one of the cases. Therefore, it is important for us *to use the same regression method for all the cases rather than to choose an optimal method*.

For studies aimed for theoretical interpretations it is better to use a linear fit that is symmetric to interchanges of the two variables, e.g. the bisector or orthogonal regression linear methods. Here we fit the correlations using the forward, backward, bisector, and orthogonal linear regression models. However, for further analysis and discussion, *we will use only the orthogonal regression results*. The origin of coordinates for each correlation is shifted to the 'barycenter' of the corresponding variables, where the slope and zero point are uncorrelated.

The corresponding linear regressions, *not taking into account* the errors in the variables, were carried out for our galaxy sample in Zavala (2003) by using the SLOPES routine (Isobe et al. 1990; Feigelson & Babu 1992). This seems to be a feasible approximation when the intrinsic scatter in the regression line dominates any errors arising from the measurement and error propagation procedures (Isobe et al. 1990). The TFR is the tightest one among the scaling relations. Studies of the TFR have shown indeed that the intrinsic scatter of the linear fit is larger than the measurement and correction errors (for both magnitude and velocity). For example, Giovanelli et al. (1997) showed that the latter errors account for  $\sim 0.25 - 0.15$  mag (from smaller to larger velocities), while the total scatter to the fit is  $\sim 0.45 - 0.30$  mag for the same range of velocities, implying that the *intrinsic* scatter dominates over the measurement and correction uncertainties. For the other scaling relations, this difference is expected to be even larger.

Since we have obtained estimates of the errors in the variables of the scaling relations (Appendix A), we carry out here the corresponding "error-in-variable" regression models. Thus, the analysis in the present paper is more exact than in Zavala (2003) and it allows us to roughly estimate the values of the intrinsic scatter in the different scaling relationships. Because the errors differ from point to point, the model should be heteroscedastic. We assume that the scaling relations have an (unknown) intrinsic scatter, which we want to estimate, explore, and confront with theory. The fitting regressions taking into account heteroscedastic measurement errors are carried out using the method and routine presented in Akritas & Bershady (1996). The total average intrinsic scatter,

TABLE 1  
LINEAR DOUBLY-WEIGHTED FIT PARAMETERS AND SCATTERS  
FOR THE TF (LOG-LOG) CORRELATIONS.

Fit	$b$	$\pm 1\sigma$	$a$	$\pm 1\sigma$	$\sigma_{\text{obs}}$	$\sigma_{\text{fit}}$	$\sigma_{\text{intr}}$
$V_m-M_{\text{bar}}$							
Forward	0.303	0.012	-0.979	0.127	0.029	0.058	0.050
Inverse	0.333	0.014	-1.300	0.151	0.031	0.063	0.055
Bisector	0.317	0.012	-1.140	0.132	0.030	0.060	0.052
Orthog.	0.306	0.012	-1.024	0.129	0.028	0.058	0.051
$V_m-M_s$							
Forward	0.274	0.011	-0.639	0.121	0.036	0.058	0.045
Inverse	0.294	0.013	-0.843	0.137	0.038	0.061	0.048
Bisector	0.284	0.012	-0.741	0.127	0.037	0.059	0.046
Orthog.	0.274	0.012	-0.650	0.123	0.035	0.058	0.045
$V_m-L_K$							
Forward	0.258	0.012	-0.503	0.126	0.014	0.052	0.050
Inverse	0.272	0.012	-0.652	0.132	0.015	0.057	0.054
Bisector	0.272	0.012	-0.652	0.132	0.014	0.054	0.052
Orthog.	0.261	0.012	-0.520	0.128	0.014	0.051	0.049
$V_m-L_B$							
Forward	0.310	0.015	-0.917	0.152	0.016	0.064	0.062
Inverse	0.361	0.016	-1.430	0.169	0.018	0.073	0.072
Bisector	0.335	0.014	-1.170	0.149	0.017	0.068	0.066
Orthog.	0.314	0.015	-0.963	0.154	0.016	0.065	0.063

NOTE. —  $\text{Log}V_m = a + b\text{Log}M(L)$ .  $V_m$  is given in  $\text{kms}^{-1}$ ,  $M_{\text{bar}}$  and  $M_s$  in  $M_\odot$ ,  $L_K$  in  $L_{K\odot}$ , and  $L_B$  in  $L_{B\odot}$ .

$\sigma_{\text{intr}}$ , is estimated as the square root of the variance of the fit,  $\sigma_{\text{fit}}^2$ , subtracted from the average (in both variables) observable variance,  $\sigma_{\text{obs}}^2$  ( $= N / \sum 1/[\sigma_y^2 + b^2\sigma_x^2]$ , where  $N$  is the number of data points and  $b$  is the slope of the correlation), i.e.,  $\sigma_{\text{intr}}^2 = \sigma_{\text{fit}}^2 - \sigma_{\text{obs}}^2$ . More elaborated fitting procedures could be used to estimate the intrinsic scatter (e.g., Gnedin et al. 2007). However, given the level of approximation we have used to determine the errors for the data, we consider that our first-order approximation is enough.

Tables 1 – 3 show the results from the different regression methods applied to the three scaling correlations in the four cases (baryonic and stellar quantities, and  $K$  and  $B$  bands). We report the zero point,  $a$ , the slope and  $b$ , with their respective standard deviations (calculated in the 'barycenter' of the variables), as well as the corresponding square roots of the variance of the fit,  $\sigma_{\text{fit}}$ , the bi-weighted average of the individual (in both variables) variances,  $\sigma_{\text{obs}}$ , and the total average intrinsic variance,  $\sigma_{\text{intr}}$ . We recall that our analysis, including the scatters, refers to the logarithm of the quantities involved. In the panels of Figs. 1 to 3, we plot the forward (dashed line), backward (dotted line), and orthogonal (solid line) doubly-weighted linear fits.

### 3.1. Luminosity (mass) vs velocity (TFRs)

As Fig. 1 and Table 1 show, the  $V_m-L_B$ ,  $V_m-L_K$ ,  $V_m-M_s$  and  $V_m-M_{\text{bar}}$  correlations are tight, although the differences between the lines obtained from the different regression methods are slightly larger than the dispersion associated to any given line. Therefore, the choice of the fitting method will affect slightly the results. For all the cases, the slopes of the forward correlations are shallower than the ones of the inverse correlations. For the bisector and orthogonal correlations, their slopes are between those of the forward and inverse correlations. The orthogonal correlations have slopes shallower than the bisector correlations, very close to the ones obtained from

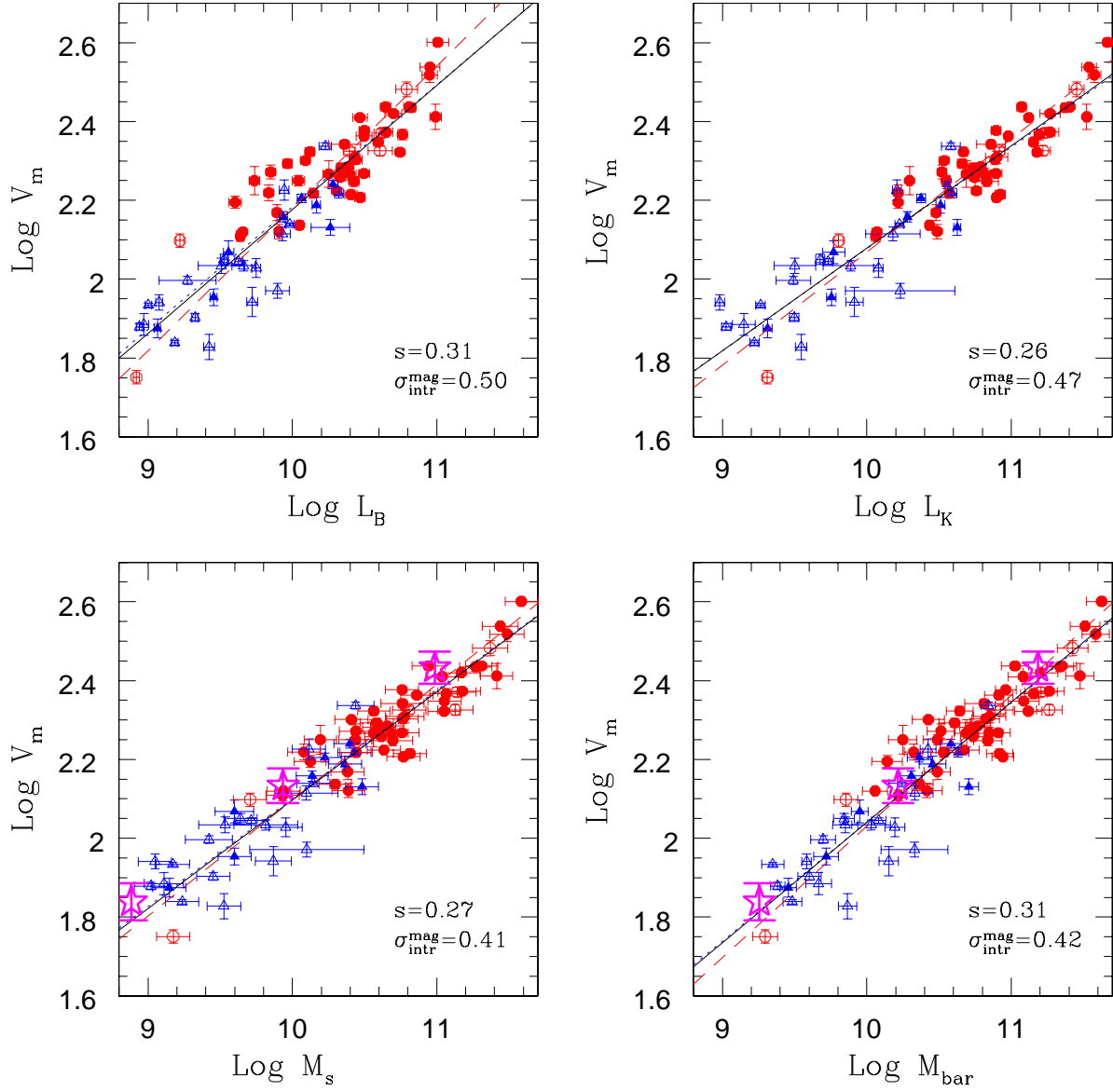


FIG. 1.— Observed TF correlations in the  $B$  and  $K$  bands (upper panels) and for stellar and baryonic masses (lower panels).  $V_m$  is in km/s and the luminosities and masses in the corresponding solar units. Solid and empty symbols are for HSB ( $\mu_{K,0} \leq 18.5$  mag/arcsec<sup>2</sup>) and LSB ( $\mu_{K,0} > 18.5$  mag/arcsec<sup>2</sup>) galaxies, respectively. Red galaxies ( $[B - K] > 3$ ) are represented with (red) circles, while blue galaxies ( $[B - K] \leq 3$ ) with (blue) triangles. The solid, dotted, and dashed lines are the corresponding orthogonal, forward, and inverse linear heteroscedastic doubly-weighted regressions, respectively. The slopes and inverse intrinsic scatters of the orthogonal fits are given inside each panel. The solid (magenta) stars with vertical error bars in the lower panels are the average values of  $V_m$  and the  $rms$  scatter for a given mass from the  $\Lambda$ CDM-based disk galaxy evolutionary models presented in FA-R ( $\sigma_8 = 1$ ). The models were rescaled to  $h = 0.7$ .

the forward fit. In the following, we analyze only the correlations fitted with the orthogonal regression method. A deep statistical analysis of each one of the correlations presented here is out of the scope of the paper.

From the baryonic  $V_m$ - $M_{\text{bar}}$  to stellar  $V_m$ - $M_s$  TFR, the slope is shallower by  $\approx 11\%$ , and the mass at  $V_m = 160$  km/s is 1.36 times (0.134 dex) smaller; for larger velocities, the mass difference becomes smaller. From  $V_m$ - $M_s$  to  $V_m$ - $L_K$ , the slope remains almost constant. From  $V_m$ - $L_K$  to  $V_m$ - $L_B$  the slope is steeper by  $\approx 20\%$ , and some segregation by color appears.

Keeping in mind that most of the previous works used to report the forward slopes of the  $L$ -( $M$ )- $V_m$  correlations, we remark that the equivalent slopes here would be the inverse of our inverse linear regressions (see Table

1): 3.00, 3.40, 3.67, and 2.77 for the baryonic, stellar,  $K$ - and  $B$ -band cases, respectively.

It should be noted that the sample used here is broad in galaxy properties and *it was not pruned to reduce the TFR scatter*. The few works that carry out analysis of samples similar to ours, although with different fitting methods, give slope values for the luminous TFRs (Kannappan, Fabricant & Franx 2002; Verheijen & Sancisi 2001; Dutton et al. 2007; Courteau et al. 2007) and for the stellar TFR (Pizagno et al. 2005; Gnedin et al. 2006) close to our estimates. The recent work by Pizagno et al. (2007), that analyzes a sample of 162 SDSS disk galaxies with  $H\alpha$  rotation curves, reports slopes of the luminous TFRs much steeper than the ones obtained here. The baryonic TFR obtained in McGaugh (2005) is shallower

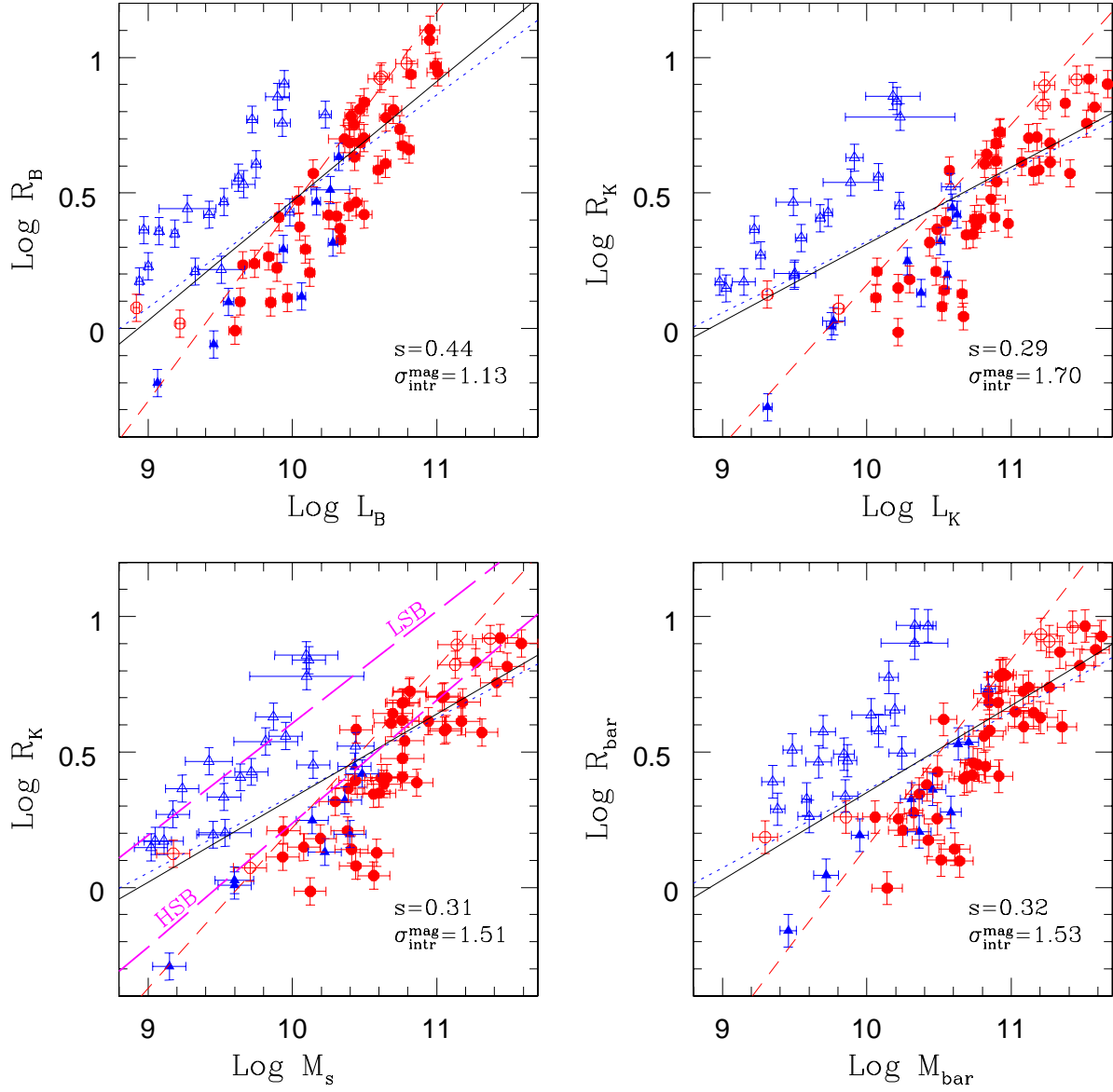


FIG. 2.— Observed radius-luminosity correlations in the  $B$  and  $K$  bands (upper panels), and radius-mass correlations for stellar and baryonic quantities (lower panels). Symbols, lines types, labels, and units are as in Fig. 1. Radii are in kpc. The thick dashed magenta lines in the  $R_K$ - $M_s$  diagram are the fits to the model LSB and HSB+very HSB galaxies presented in FA-R (rescaled to  $h = 0.7$ ).

than ours, however, he uses  $V_{\text{flat}}$  instead of  $V_m$ .

The estimated average intrinsic scatters,  $\sigma_{\text{intr}}(\text{Log} V_m)$ , in the  $V_m$ - $M_{\text{bar}}$ ,  $V_m$ - $M_s$ ,  $V_m$ - $L_K$ , and  $V_m$ - $L_B$  correlations are 0.051, 0.045, 0.049 and 0.063 dex, respectively. The intrinsic scatter is larger (by  $\sim 10\%$ ) for the baryonic correlation than for the stellar one; the largest scatter is in the  $B$ -band. The intrinsic scatter along the  $M$  or  $L$  axis expressed in magnitudes,  $\sigma_{\text{intr}}^{\text{mag}} = 2.5 \times \sigma_{\text{intr}}(\text{Log} V_m)/b$ , oscillates between 0.41 mag (stellar correlation) and 0.5 mag ( $B$  band correlation) for all the regression methods used here (see values for the orthogonal fit in Fig. 1).

Recall that our observational error estimates and their propagation are approximations. Nonetheless, our estimates for the intrinsic scatter agree with other similar works. For example, Dutton et al. (2007) estimate  $\sigma_{\text{intr}}(\text{Log} V_m) \approx 0.052$  in the  $I$ -band, in between of our values in the  $B$  and  $K$  bands. Pizagno et al. (2007), who carried out a deep analysis of the errors for their sample, find typical values of the intrinsic scatter for the opti-

cal/NIR TFRs of 0.40–0.45 mag, close to our findings.

### 3.2. Radius vs luminosity (mass)

The  $R_B$ - $L_B$ ,  $R_K$ - $L_K$ ,  $R_s$ - $M_s$ , and  $R_{\text{bar}}$ - $M_{\text{bar}}$  correlations are scattered and strongly segregated by disk central SB (Fig. 2; Table 2). For a given luminosity or mass, the disk scale length, or central SB, span a large range of values. We see from Fig. 2 that a segregation by color is also present. There is no significant difference between the slopes and zero points of the baryonic and stellar  $R$ - $M$  correlations. Both the mass and the radius increase when changing from stellar to baryon quantities, but the change is small and shifts galaxies along the same correlation, whose slope is  $\approx 0.32$ . From the stellar to the  $K$ -band correlation, the slope slightly decreases, while from the  $K$ - to the  $B$ -band correlation the slope strongly increases, from  $0.28 \pm 0.03$  to  $0.44 \pm 0.04$ .

The intrinsic scatter measured in the Log of the radii is approximately the same in all the cases,  $\sigma_{\text{intr}}(\text{Log} R) \approx$

TABLE 2  
LINEAR DOUBLY-WEIGHTED PARAMETERS AND SCATTERS FOR  
THE RADIUS–MASS (LUMINOSITY) (LOG-LOG) RELATIONS

Fit	$b$	$\pm 1\sigma$	$a$	$\pm 1\sigma$	$\sigma_{\text{obs}}$	$\sigma_{\text{fit}}$	$\sigma_{\text{intr}}$
$R_{\text{bar}}-M_{\text{bar}}$							
Forward	0.287	0.035	-2.510	0.379	0.065	0.207	0.196
Inverse	0.692	0.098	-6.770	1.030	0.085	0.032	0.313
Bisector	0.474	0.042	-4.470	0.444	0.073	0.236	0.225
Orthog.	0.322	0.039	-2.870	0.422	0.067	0.208	0.197
$R_s-M_s$							
Forward	0.285	0.031	-2.510	0.327	0.061	0.196	0.187
Inverse	0.592	0.073	-5.700	0.765	0.087	0.282	0.269
Bisector	0.430	0.034	-4.020	0.366	0.072	0.218	0.206
Orthog.	0.310	0.033	-2.770	0.352	0.063	0.196	0.187
$R_K-L_K$							
Forward	0.262	0.030	-2.300	0.324	0.052	0.201	0.194
Inverse	0.593	0.075	-5.770	0.794	0.056	0.294	0.289
Bisector	0.418	0.035	-3.940	0.378	0.054	0.223	0.217
Orthog.	0.285	0.033	-2.540	0.355	0.052	0.201	0.194
$R_B-L_B$							
Forward	0.393	0.039	-3.460	0.403	0.053	0.206	0.198
Inverse	0.718	0.065	-6.730	0.658	0.058	0.278	0.271
Bisector	0.545	0.037	-4.980	0.387	0.055	0.223	0.216
Orthog.	0.441	0.044	-3.940	0.452	0.054	0.207	0.200

NOTE. —  $\text{Log}R = a + b\text{Log}M(L)$ . The radii are given in kpc,  $M_{\text{bar}}$  and  $M_s$  in  $M_\odot$ ,  $L_K$  in  $L_{K\odot}$ , and  $L_B$  in  $L_{B\odot}$ .

TABLE 3  
LINEAR DOUBLY-WEIGHTED REGRESSION PARAMETERS AND  
SCATTERS FOR THE  $V_m$ -RADIUS (LOG-LOG) RELATIONS

Fit	$b$	$\pm 1\sigma$	$a$	$\pm 1\sigma$	$\sigma_{\text{obs}}$	$\sigma_{\text{fit}}$	$\sigma_{\text{intr}}$
$V_m-R_{\text{bar}}$							
Forward	0.332	0.078	2.030	0.044	0.024	0.160	0.158
Inverse	1.520	0.318	1.420	0.174	0.093	0.359	0.348
Bisector	0.768	0.056	1.810	0.044	0.048	0.201	0.195
Orthog.	0.506	0.109	1.937	0.063	0.033	0.167	0.164
$V_m-R_K$							
Forward	0.390	0.068	2.030	0.035	0.024	0.149	0.147
Inverse	1.220	0.196	1.670	0.096	0.063	0.274	0.267
Bisector	0.727	0.053	1.880	0.037	0.039	0.177	0.172
Orthog.	0.534	0.085	1.970	0.046	0.030	0.155	0.152
$V_m-R_B$							
Forward	0.378	0.057	2.010	0.035	0.023	0.142	0.140
Inverse	1.050	0.157	1.680	0.088	0.055	0.257	0.241
Bisector	0.662	0.049	1.870	0.038	0.036	0.167	0.163
Orthog.	0.481	0.067	1.960	0.043	0.028	0.146	0.143

NOTE. —  $\text{Log}V_m = a + b\text{Log}R$ .  $V_m$  is given in  $\text{kms}^{-1}$ , and the radii in kpc.

0.2. When translated to the ( $X$ -axis) scatter in  $\text{Log}L$  or  $\text{Log}M$  and expressed in magnitudes, the scatter is around 1.1 mag for the  $B$ -band correlation and 1.5–1.7 mag for the other correlations. Hence, in the  $B$  band, the dispersion along the luminosity is decreased by some compensation effect. The observational errors in the  $R$ - $L$  ( $-M$ ) diagrams are significantly smaller than the corresponding average intrinsic scatters. Notice that, contrary to the TFRs, for the  $R$ - $L$  ( $-M$ ) correlations, the use of a broad range in SBs (from HSB to LSB galaxies) spreads significantly the correlation and influences the slope and zero-point values. This can be clearly appreciated in Fig. 2: if we exclude the LSB galaxies, then the fit changes notably. In most of the previous works aimed to estimate the disk scaling relations, *LSB galaxies were not considered. This is unfortunate if the observations are to be*

*used to compare and constrain theoretical models.*

### 3.3. Velocity vs radius

The  $V_m-R_B$ ,  $V_m-R_K$ , and  $V_m-R_{\text{bar}}$  correlations are shown in Fig. 3 and their fitting parameters are given in Table 3. The  $V_m-R_s$  correlation is the same as the  $V_m-R_K$  one because we assumed that  $R_s = R_K$ . The  $V_m-R$  correlations are highly scattered, and segregated by disk surface brightness and color. For these correlations, the differences between forward and inverse fits are large. The relative errors in the fitted slope and zero point parameters are the largest ones among the three scaling relations studied here.

Because of the large dispersions in the fitted slopes and zero points of the  $V_m-R$  correlations, there is no significant difference among these parameters when we change from the  $B$  to the  $K$  band and to the baryonic case. For the orthogonal regression, the slopes and zero points are  $\approx 0.5$  and  $\approx 1.95$ , respectively. The intrinsic scatter slightly decreases from the baryonic to the  $K$ -band,  $\sigma_{\text{intr}}(\text{Log}V_m) \approx 0.17$  and 0.15, respectively. The estimated inverse intrinsic scatter (along the  $L$  axis) increases from the  $K$  to the  $B$  band.

### 3.4. Other global correlations

In order to complement the presented scaling correlations and their changes when moving from luminous to stellar and baryonic quantities, we explored the possibility of other correlations for our galaxy sample involving luminosities (masses), global color, central surface densities (brightnesses), and stellar mass content. Fig. 4 shows the  $(B-K)$  color vs  $L_B$ ,  $L_K$ ,  $M_s$ , and  $M_{\text{bar}}$ , with the corresponding Pearson correlation coefficients and slopes. In spite of the  $L$ -dependent correction by internal extinction that we have applied, a clear correlation of color with  $L$  and  $M$  remains: more massive (luminous) galaxies are on average redder than the less massive (luminous) ones. The  $B$ -band correlation is the most scattered, as expected. The slope becomes slightly steeper when changing from  $M_s$  to  $M_{\text{bar}}$  mainly because the less massive, bluer galaxies have typically larger gas mass fractions, shifting then more to the right side in the  $\text{Log}M$  axis than the massive galaxies. The slope also becomes steeper when changing from  $L_K$  to  $L_B$ , in this case just because less luminous galaxies being bluer on average, shift more to the right side in the  $\text{Log}L$  axis than the redder luminous galaxies.

Noisy Log-Log correlations are observed also between  $(B-K)$  and the different SBs and surface densities, and between the latter quantities and the luminosities and masses (Fig. 5). The slopes of the orthogonal fits are given inside each corresponding panel. The general trend is that the higher the surface density (SB), the redder and more massive (luminous) is the galaxy. What lies at the basis of these trends for disk galaxies? We have also explored correlations related to the galaxy stellar mass fraction,  $f_s$  (or gas mass fraction  $f_g = 1 - f_s$ ). This quantity is an important property of galaxies related to their gas infall and SF rate histories; it will be discussed in §4.2 (see Fig. 7 therein). The fraction  $f_s$  correlates strongly with the  $(B-K)$  color and weakly with the surface densities (SBs) and luminosities (masses), in that order. For all cases, the lowest SB galaxies break the correlations, suggesting a kind of a threshold for the



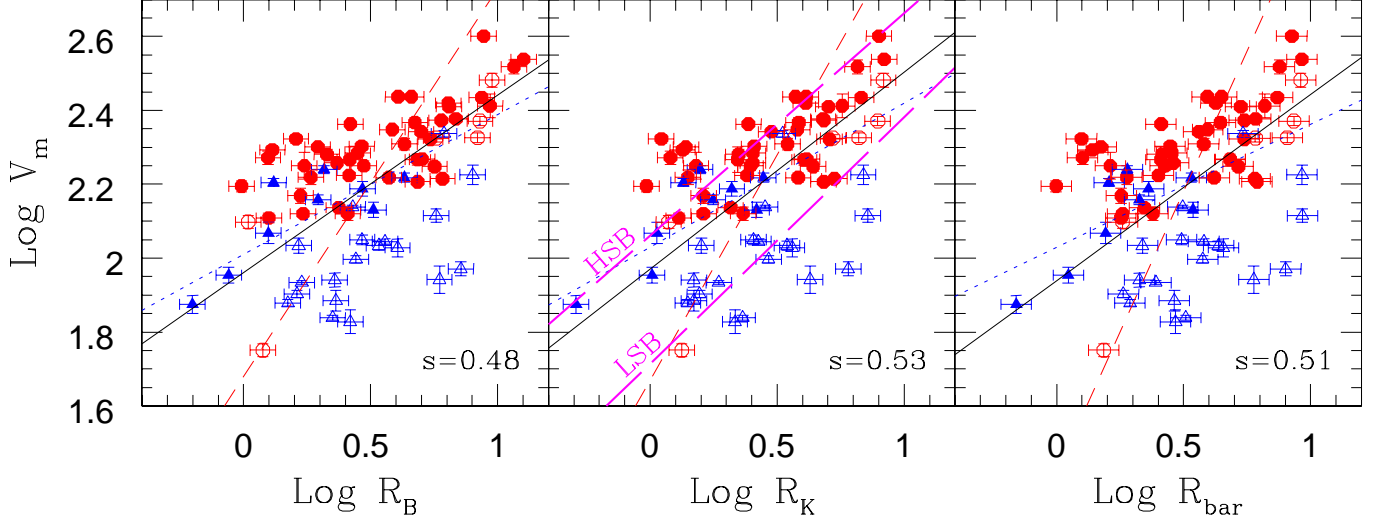


FIG. 3.— Observed  $V_m$ -radius correlations in the  $B$  and  $K$  bands (left and mid panels), and baryonic  $V_m$ - $R_{\text{bar}}$  correlation (right panel). Because we assumed  $R_s=R_K$ , the stellar  $V_m$ - $R_s$  correlation is as the  $V_m$ - $R_K$  one. Symbols, line types and labels are as in Fig. 1. The thick dashed magenta lines are the fits to the model LSB and HSB+very HSB galaxies presented in FA-R (rescaled to  $h=0.7$ ).

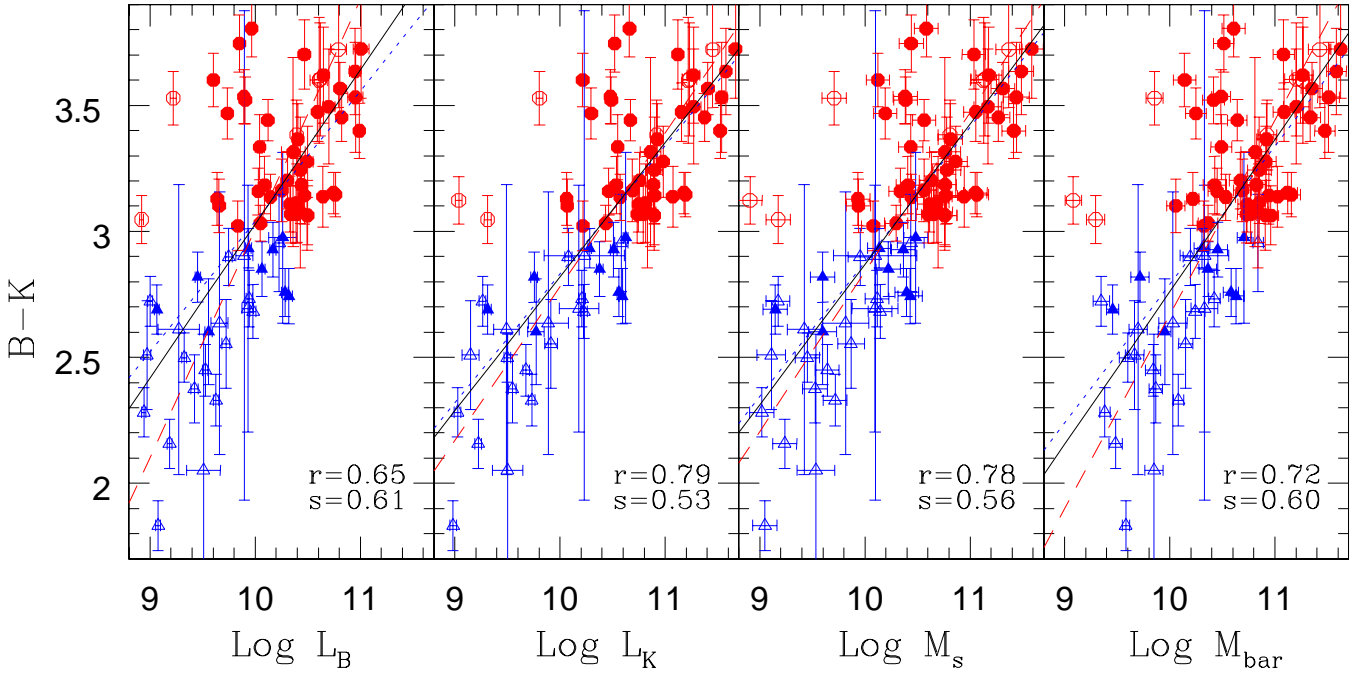


FIG. 4.— Corrected  $(B-K)$  color vs the logarithms of  $L_B$ ,  $L_K$ ,  $M_s$ , and  $M_{\text{bar}}$ . Symbols and line types are as in Fig. 1. The Pearson's correlation coefficient,  $r$ , and the slope of the orthogonal fit,  $s$ , appear in the right-bottom corner of each panel.

surface density, below which the SF efficiency is almost independent of it (and of  $M$  or  $L$ ).

### 3.5. Residual correlations and the search for other significant parameters in the scaling relations

To gain a more quantitative description of the disk galaxy scaling relations and their implications, we may explore the behavior of their residuals. The possible correlations of the residuals among them, and other galaxy properties, bring valuable information on galaxy formation and evolution processes. In particular, the changes of the residual correlations when moving from optical to NIR bands and to stellar and baryonic quantities provide

clues on the SF and stellar population evolution processes as well as on the dynamics of disk galaxies.

In the different panels of Fig. 6, the residuals of the  $V_m$ - $M$ (- $L$ ) correlations are plotted against the corresponding residuals of the  $R$ - $M$ (- $L$ ),  $(B-K)$ - $M$ (- $L$ ), and  $f_s$ - $M$ (- $L$ ) correlations for the baryonic, stellar,  $K$ - and  $B$ -band cases, respectively. The orthogonal regression fit was used to obtain the residuals. As can be seen in Fig. 6, for most of the cases, the residuals are weakly correlated or completely uncorrelated with each other.

For the baryonic case, we find an anti-correlation of  $\Delta V_m(M_{\text{bar}})$  with  $\Delta R_{\text{bar}}(M_{\text{bar}})$  with slope  $-0.15 \pm 0.04$  (orthogonal linear regression): on average, the more a

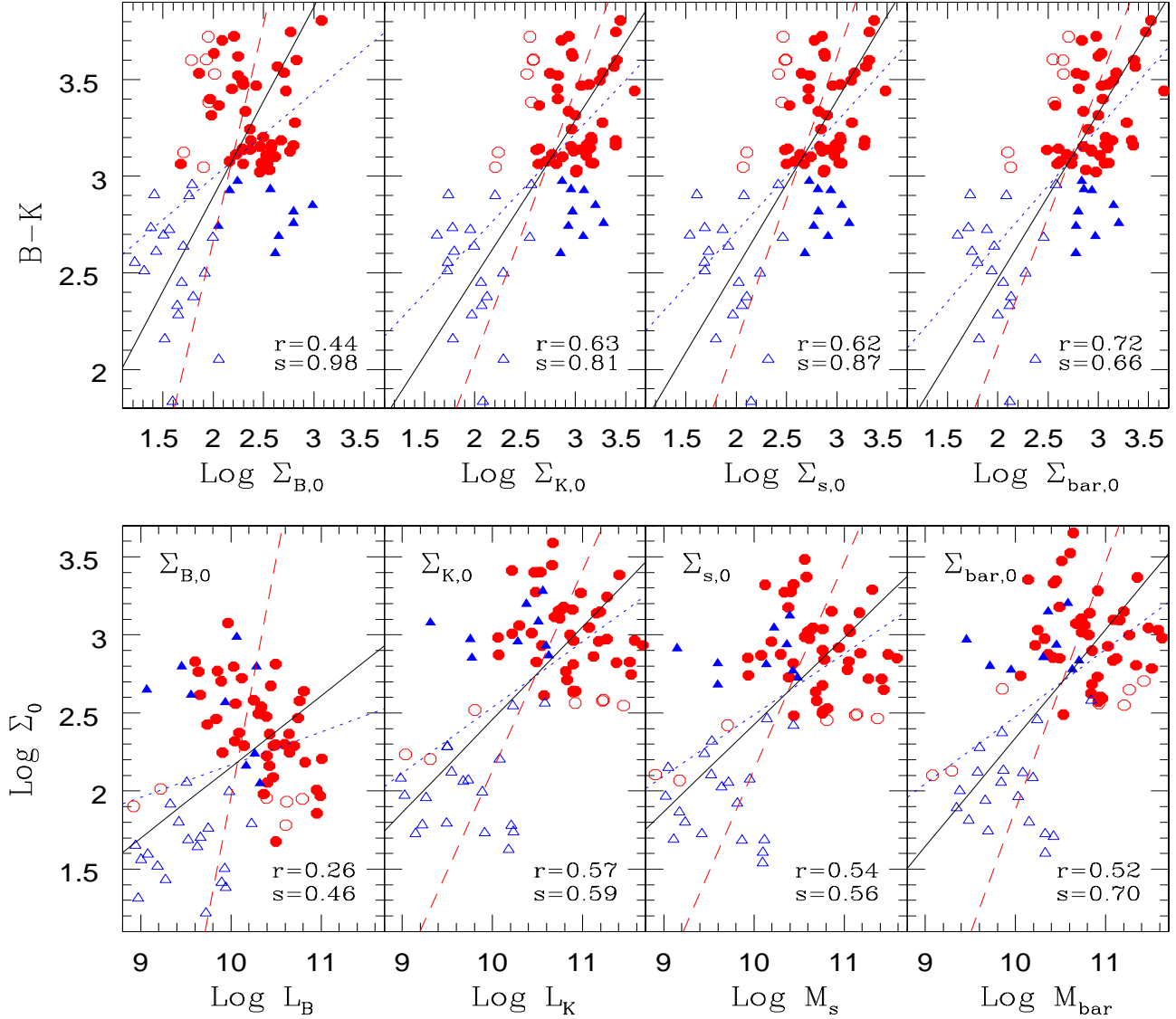


FIG. 5.— Corrected  $(B-K)$  color vs the Log of  $\Sigma_{B,0}$ ,  $\Sigma_{K,0}$ ,  $\Sigma_{s,0}$  and  $\Sigma_{bar,0}$  (top panels), and  $\text{Log } \Sigma_0$  vs  $\text{Log}(M, L)$  for B, K bands, stellar and baryonic components from left to right (bottom panels). Symbols and line types are as in Fig. 1. Labels are as in Fig. 4.

galaxy deviates in the direction of the high-velocity side in the  $V_m$ - $M_{bar}$  relation, the more it deviates in the direction of the small-radius side in the  $R_{bar}$ - $M_{bar}$  relation. It is illustrative to know that for the extreme case of exponential disks without dark matter halos, the slope would be  $-0.5$ , while for completely halo dominated galaxies, no correlation is expected. For the stellar and  $K$ - and  $B$ -band cases, the trend described above almost disappears. These results show that *the residuals of the  $V_m$ - $L$  ( $-M$ ) and  $R$ - $L$  ( $-M$ ) correlations can or cannot correlate, depending not only on the inner dynamics of the galaxies themselves, but also on their SF histories, a question highlighted in FA-R*. From the left column of Fig. 6, we learn also that for all cases, the LSB galaxies are more scattered and uncorrelated than the HSB ones in the residuals plane.

As expected, the residuals of the  $R$ - $L$  ( $-M$ ) correlations anti-correlate strongly with the corresponding disk central surface densities (or SBs) as:  $\Delta R_{bar}(M_{bar}) \propto$

$\Sigma_{bar,0}^{-0.34}$ ,  $\Delta R_s(M_s) \propto \Sigma_{s,0}^{-0.39}$ ,  $\Delta R_K(L_K) \propto \Sigma_{K,0}^{-0.37}$ , and  $\Delta R_B(L_B) \propto \Sigma_{B,0}^{-0.45}$ . The surface density (or SB) is clearly a significant third parameter in all the  $R$ - $L$  ( $-M$ ) correlations. The tightest anti-correlation is for the baryonic case; then its strength decreases successively for the stellar,  $K$ -band, and  $B$ -band cases. The residuals of the  $V_m$ - $R$  correlations correlate significantly with the corresponding surface densities (SBs). These residuals also correlate with those of the  $V_m$ - $L$  ( $-M$ ) correlations, but with a considerable segregation by SB, resembling the  $R$ - $L$  ( $-M$ ) correlations.

The findings reported above imply that the radius could be a statistically significant third parameter in the baryonic TFR. Applying a backward step-wise multiple linear regression procedure, where  $F$  tests are used to compute the significance of each independent variable<sup>7</sup>,

<sup>7</sup> In this analysis,  $V_m$  is assumed to be the dependent variable and  $M$  (or  $L$ ),  $\Sigma_0$ ,  $R$ ,  $(B-K)$ ,  $f_g$ , and the morphological type  $T$  are

Zavala (2003) has indeed found that the radius is a third (statistically significant) parameter in the baryonic TFR. However, the radius was not found to be anymore a third parameter in the stellar and luminous TFRs. We confirm here the results by Zavala (2003), with the exception that for our analysis in the  $B$  band, the radius is statistically more significant than in the analysis of Zavala (2003), however, we still find that the radius is not a third parameter in the  $B$ -band TFR; instead, the  $(B-K)$  color is a third parameter in this case.

Since we are interested in the changes in the scaling correlations when changing from one band to another and to stellar and baryonic quantities, it is important then to analyze also the possible dependencies of their residuals on galaxy color and stellar fraction. In the mid and right panels of Fig. 6, the residuals of the  $V_m$ - $L$  ( $-M$ ) correlations are plotted vs the residuals of the  $(B-K)$ - $L$  ( $-M$ ) and  $f_s$ - $L$  ( $-M$ ) correlations, rather than just vs  $(B-K)$  and  $f_s$ . In this way, the comparisons are at a given  $L$  or  $M$ . In the baryonic case, there are noisy trends: the residuals of the  $V_m$ - $M_{\text{bar}}$  correlation increase on average for increasing residuals of the  $(B-K)$ - $M_{\text{bar}}$  and  $f_s$ - $M_{\text{bar}}$  correlations (the galaxies become redder and with higher  $f_s$ ); however, this is only true for the HSB galaxies. In the stellar and  $K$ -band cases, one does not see any clear trend. In the  $B$  band, the residuals  $\Delta V_m(L_B)$  correlate with the residuals  $\Delta(B-K)(L_B)$ , although mainly due to the HSB galaxies. The backward step-wise analysis shows that the  $(B-K)$  color is indeed the third parameter in the  $B$ -band TFR (see also Kannappan et al. 2002; Pizagno et al. 2007; Courteau et al. 2007). There is also a weak correlation of  $\Delta V_m(L_B)$  with  $\Delta f_s(L_B)$ .

#### 4. INTERPRETING THE SCALING RELATIONS

The results reported in §3 reveal non-negligible changes in the slopes and scatters of the scaling correlations of disk galaxies when changing from  $B$  to  $K$  bands and to stellar and baryonic quantities. While the most robust aspects of the scaling relations seem to be a consequence of the cosmological initial conditions of disk galaxy formation (e.g., FA-R; Shen et al. 2001; Dutton et al. 2007), the changes found here are expected to be related mainly with the SF and gas infall histories of galaxies. In the following, we focus our discussion on the findings presented in §3 and on whether or not these changes are expected in  $\Lambda$ CDM-based models of disk galaxy evolution.

##### 4.1. The baryonic relations

The scenario of disk galaxy formation sketched in Appendix B makes certain predictions regarding the baryonic scaling relations of disk galaxies (Appendix C). The main simple physical ingredients of disk galaxy formation and evolution are the halo mass  $M_h$ , the mass assembly history (MAH), the spin parameter  $\lambda$ , and the disk galaxy mass fraction  $f_{\text{gal}} \equiv M_{\text{bar}}/M_h$ . Below, we highlight some of the main aspects of these predictions

the independent variables. For each case (baryonic, stellar, and  $B$  and  $K$  bands), one starts from a multiple variable linear regression using *all* the variables and then, through the backward step-wise procedure, the variables that are not statistically significant are eliminated step by step.

with the goal of interpreting the observational inferences presented in §3. At some points, we will discuss in more detail the model results obtained in FA-R. In that work, the cosmology used corresponded to a flat  $\Lambda$ CDM universe with  $\Omega_{M,0} = 0.35$ ,  $\Omega_\Lambda = 0.65$ ,  $h = 0.65$ ,  $\sigma_8 = 1$ ;  $f_{\text{gal}}$  was assumed to be constant.

**The  $V_m$ - $M_{\text{bar}}$  relation.** As described in the Appendix C1, if the initial condition parameters  $\lambda$  and  $f_{\text{gal}}$  do not depend significantly on mass, then one expects that the baryonic TFR should have a slope similar to the cosmological one. *This seems to be the case according to our results* ( $a_{\text{bar}} \approx 0.31$  from observation vs  $a_{\text{halo}} = 0.30 - 0.32$  from simulations). The models of FA-R and Dutton et al. (2007) show that for a reasonable range of  $f_{\text{gal}}$  values (between  $\sim 0.03 - 0.08$ ), changes of  $f_{\text{gal}}$  with mass would not have a significant effect on the baryonic TFR slope (taking into account the disk gravitational drag on the halo); for a given  $M_h$ , as  $f_{\text{gal}}$  decreases,  $M_{\text{bar}}$  decreases, but  $V_m$  also decreases (actually is the  $G$  function defined in the Appendix C1 that decreases), and the galaxy model shifts along the relation. In the same way, a moderate correlation (anti-correlation) of  $\lambda$  with mass would only decrease (increase) slightly the slope. Conversely, steep dependencies of  $f_{\text{gal}}$  and/or  $\lambda$  upon mass would imply a significant change in the slope of the TFR.

Regarding the intrinsic scatter, we have measured from the observational sample a value of  $\sigma_{\text{intr}}(\text{Log} V_m) = 0.051$  for the baryonic TFR. This value, in spite of the broadness of the sample, *is in marginal agreement with the theoretical expectations discussed in Appendix C1*. For example, for the FA-R models with  $f_{\text{gal}} = 0.05$ ,  $\sigma_{\text{intr}}(\text{Log} V_m) \approx 0.053$ ; by relaxing some models assumptions, this value is expected to be larger. Thus, from the comparison of observations with theory, it seems that there is no room for other significant sources of scatter, either physical or systematical, as for example disk ellipticity and non-circular motions (see §5 for further discussion).

Further pieces of information related to the scatter in the baryonic TFR are given by the correlations between the residuals of this relation,  $\Delta V_m(M_{\text{bar}})$ , and those of the  $R_{\text{bar}}$ - $M_{\text{bar}}$ ,  $(B-K)$ - $M_{\text{bar}}$  and  $f_s$ - $M_{\text{bar}}$  correlations (Fig. 6). The fact that  $\Delta V_m(M_{\text{bar}})$  anti-correlates with  $\Delta R_{\text{bar}}(M_{\text{bar}})$  shows that *the radius (or surface density) plays a role in the scatter of the baryonic TFR*. As mentioned in §3.5, the radius is found to be indeed a statistically significant parameter in the  $V_m$ - $M_{\text{bar}}$ - $R_{\text{bar}}$  multi-variable correlation. Because  $\Delta R_{\text{bar}}(M_{\text{bar}})$  correlates strongly with  $\Sigma_{\text{bar},0}$  (§3.5), the anti-correlation seen in Fig. 6 implies that, for a given  $M_{\text{bar}}$ , higher surface density disks produce larger values of  $V_m$ . For a given  $\lambda$  distribution, the larger  $f_{\text{gal}}$ , the higher the disk surface density, and hence the more pronounced is the effect upon  $V_m$  because the disk contribution to the total rotation curve is larger. This implies a steeper and stronger anti-correlation between  $\Delta V_m(M_{\text{bar}})$  and  $\Delta R_{\text{bar}}(M_{\text{bar}})$ . In the extreme case of complete dominion of an exponential disks (no dark matter halo), this anti-correlation should have a slope of  $-0.5$  (Courteau & Rix 1999).

Our observational results point out to a slope shallower than  $-0.5$ ,  $\approx -0.15$ , *showing that the dark halo contribution at a radius where the rotational velocity is maximal, is significant*, as predicted by models based

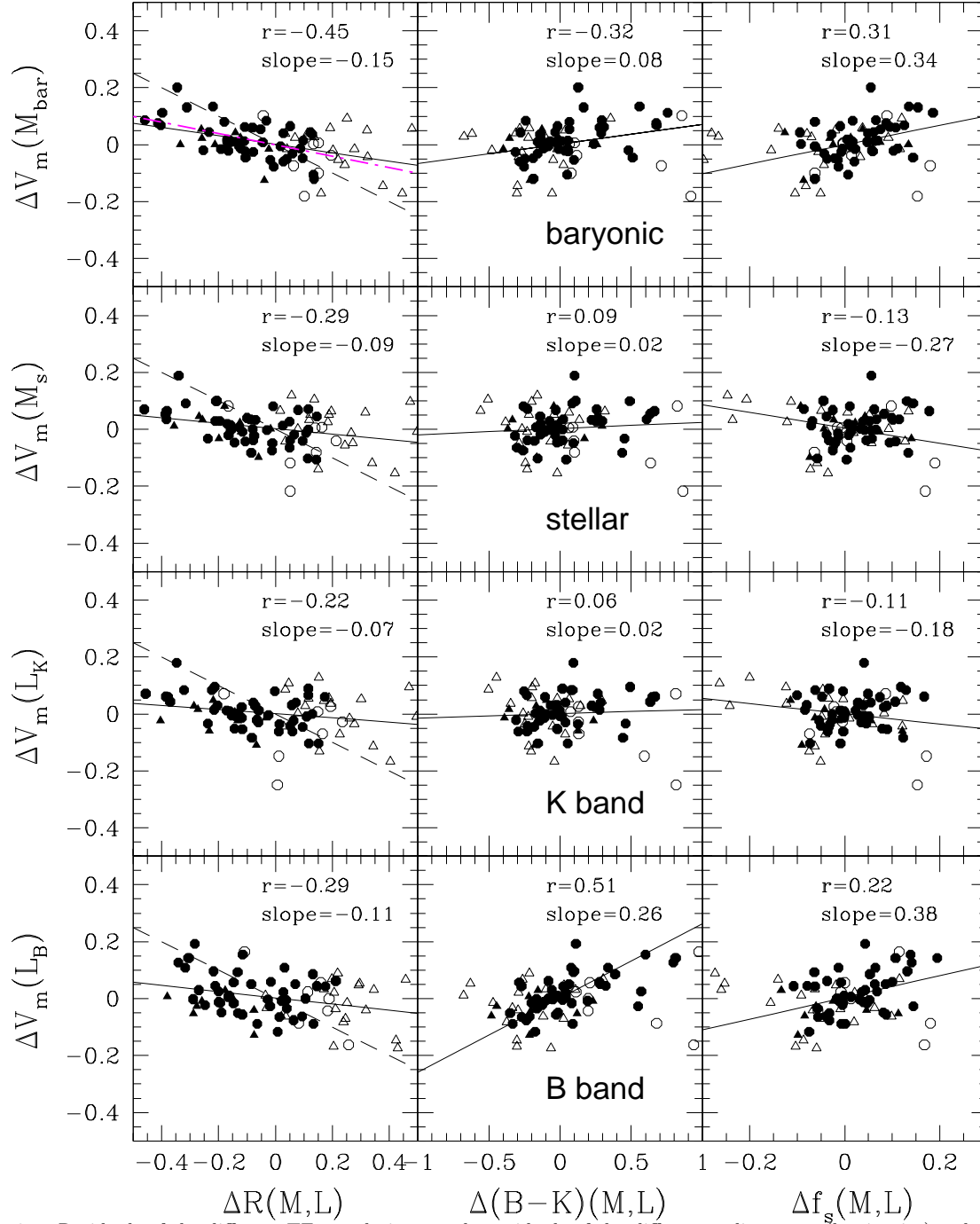


FIG. 6.— Residuals of the different TF correlations vs the residuals of the different radius-mass (luminosity), color-mass (luminosity), and  $f_s$ -mass (luminosity) correlations. From top to bottom, the rows correspond to the baryonic, stellar,  $K$  and  $B$  band cases. Symbols are as in Fig. 1. The solid lines are the orthogonal linear regressions. The corresponding Pearson correlation coefficients and the slopes are given inside each panel. The dot-dashed (magenta) line in the upper left panel is the linear fit to the model results by FA-R. The dashed lines in all the panels of the left column indicate the prediction for an exponential disk without dark halo (slope = -0.5).

on  $\Lambda$ CDM halos. According to Fig. 6, the residuals are more tightly anti-correlated for the HSB sub-sample than for the LSB one. This implies that the dark halo component becomes more dominant for lower values of the disk SB, to the point that the contribution of the disk to the total rotation curve at radii close to its maximum, is negligible for the lowest SB galaxies. This dependence of the baryon and dark matter contents with SB has been deeply explored in ZAHF, who showed for the same galaxy sample used here that only the highest SB disk galaxies are maximum disk, while the lower

the SB, the more dark-halo-dominated (sub-maximum disk) the galaxies become (see also e.g., Casertano & van Gorkom 1991; de Blok & Bosma 2002; Catinella et al. 2007). It is important to mention that the slope of the residual correlation is sensitive to  $f_{\text{gal}}$ . For the modeling of disks formed inside  $\Lambda$ CDM halos discussed above, the slope will be significantly steeper than -0.15 if the average value of  $f_{\text{gal}}$  is larger than 0.05 (e.g., Gnedin et al. 2007; Dutton et al. 2007; Pizagno et al. 2007). For the cosmology used by FA-R and  $f_{\text{gal}}=0.05$ , they found that the slope is  $\approx -0.20$  (see their Fig. 8). An

interesting question is *what slope would be predicted by alternative theories, like the Modified Newtonian Dynamics, and whether it would agree with the value of  $\approx -0.15$  found here using a broad sample of disk galaxies.*

We stress that observational studies aimed to constrain the baryon and dark matter contents in disk galaxies should use the baryonic relations instead of the luminous or stellar ones. For example Courteau & Rix (1999) obtained the residuals of the observed (infrared) TFR and  $R$ - $L$  relation for a sample of mostly HSB galaxies, and interpreted the lack of correlation between these residuals as evidence of dark matter dominance in all galaxies. As FA-R showed, the dependency among the residuals changes from the baryonic to the stellar relations (see also Dutton et al. 2007; Courteau et al. 2007). Our observational results confirm this fine effect.

**The  $R_{\text{bar}}$ - $M_{\text{bar}}$  relation.** For the galaxy sample analyzed here, the  $R_{\text{bar}}$ - $M_{\text{bar}}$  correlation is highly scattered ( $\sigma_{\text{intr}}(\text{Log}R) = 0.2$  for the orthogonal fit), with the scatter indeed anti-correlating strongly with  $\Sigma_{\text{bar},0}$  ( $r = -0.91$ ), and less with the  $(B - K)$  color, as the  $\Lambda$ CDM-based models predict (Appendix C2). The slope of the correlation, for the orthogonal fit, is  $0.32 \pm 0.04$  (Table 2) and is steeper for the bisector and inverse fits, i.e. is close to the slope of the CDM halo  $R_{\text{h}}$ - $M_{\text{h}}$  relation (Appendix B). *Thus, according to the arguments given in Appendix C2, there is almost no room for a significant dependence of  $\lambda$  or  $f_{\text{gal}}$  on  $M_{\text{bar}}$ , in the range of masses of the galaxies studied here, although if both parameters anti-correlate (or correlate) at the same time with  $M_{\text{bar}}$  then the slope changes may be compensated.*

**The  $V_{\text{m}}$ - $R_{\text{bar}}$  relation.** The slope of the (noisy)  $V_{\text{m}}$ - $R_{\text{bar}}$  correlation found here is  $0.51 \pm 0.11$  (orthogonal fit), i.e. shallower than the cosmological one (see Appendix B). This, according to Appendix C3 *favours, if any, an anti-correlation of  $f_{\text{gal}}$  with mass.* The intrinsic scatter,  $\sigma_{\text{intr}}(\text{Log}V_{\text{m}}) = 0.16$ , is much larger than the scatter around the baryonic TFR. As predicted by the models, the residuals of the  $V_{\text{m}}$ - $R_{\text{bar}}$  correlation correlate significantly with both  $\log\Sigma_{\text{bar},0}$  and the  $(B - K)$  color ( $r = 0.95$  and  $0.67$ , respectively); the slopes of these correlations (orthogonal fit) are  $0.34$  and  $0.28$ , respectively.

#### 4.2. The stellar relations

The main changes when moving from the baryonic to the stellar scaling correlations are the decrease of the slope and intrinsic scatter in the  $V_{\text{m}}$ - $M$  correlations. The scatters of the  $R$ - $M$  and  $R$ - $V_{\text{m}}$  correlations also decrease but the significance of this decrement are very marginal. More interesting, the (weak) anti-correlation between the residuals of the baryonic  $V_{\text{m}}$ - $M_{\text{bar}}$  and  $R_{\text{bar}}$ - $M_{\text{bar}}$  correlations tends to disappear in the stellar case. This is a fact related to other of our results, namely that *the radius (or disk surface density) is a third parameter in the baryonic TFR but not anymore in the stellar one.* All these differences are related to the gas (or stellar) mass fraction of galaxies, and they show that the mass infall and SF histories vary systematically among galaxies. Are these variations consistent with galaxy models based on the  $\Lambda$ CDM framework?

Let us first discuss the change in the slope of the  $V_{\text{m}}$ - $M$  relation. If the stellar mass fraction,  $f_{\text{s}} = 1 - f_{\text{g}}$ , depends on  $M_{\text{s}}$  as  $f_{\text{s}} \propto M_{\text{s}}^{\beta}$ , then  $M_{\text{bar}} = M_{\text{s}}/f_{\text{s}} \propto$

$M_{\text{s}}^{1-\beta}$ . Therefore, from  $V_{\text{m}} \propto M_{\text{bar}}^{\alpha}$  one passes to  $V_{\text{m}} \propto M_{\text{s}}^{\alpha(1-\beta)}$ . In the left panel of Fig. 7, we show  $f_{\text{s}}$  vs  $M_{\text{s}}$  for our galaxy sample. Although with a high scatter,  $f_{\text{s}}$  correlates with  $M_{\text{s}}$  roughly as

$$f_{\text{s}} = 0.65(M_{\text{s}}/10^{10}M_{\odot})^{0.13}, \quad (4)$$

implying then that the slope from the baryonic to stellar TFRs should decrease by a factor  $\sim 0.87$ . The corresponding slopes calculated with the orthogonal fits are  $0.31$  and  $0.27$ , respectively. What does cause the dependence of  $f_{\text{s}}$  (or  $f_{\text{g}}$ ) on  $M_{\text{s}}$ ? It could be that rather than a fundamental dependence, it is a consequence of other correlations. For example, Fig. 7 shows that  $f_{\text{s}}$  correlates stronger with  $\Sigma_{\text{s},0}$  (and also with galaxy color) than with  $M_{\text{s}}$ .

From the point of view of the models, the stellar fraction  $f_{\text{s}}$  of normal disk galaxies depends mainly on two factors: the efficiency of gas transformation into stars, given basically by the disk surface density (determined by  $\lambda$ ,  $f_{\text{gal}}$ , and  $M_{\text{h}}$ ), and the gas infall history, connected to the halo MAH. Based on these processes and by means of semi-numerical models, FA-R and Avila-Reese & Firmani (2000) have shown that (i) lower surface density disks transform gas into stars with less efficiency than disks of high surface density, (ii) more massive disks tend to be of higher surface density (see also Dalcanton et al. 1997), and (iii) the present-day  $f_{\text{s}}$  correlates significantly with  $\Sigma_{\text{s},0}$  (or  $\Sigma_{\text{B},0}$ ), and because of item (ii), with  $M_{\text{s}}$ . Note that the dependence of  $f_{\text{s}}$  on  $\Sigma_{\text{s},0}$  is a non trivial prediction because several physical/evolutionary processes combine to give rise to the stellar (or gas) mass fraction and surface density (brightness) of evolved disk galaxies. In Fig. 7, together with the observational inferences, the model predictions presented in FA-R are plotted in the  $f_{\text{s}}$ - $\Sigma_{\text{s},0}$  diagram (magenta stars). Models and observations occupy the same region, though the models have on average slightly lower  $f_{\text{s}}$  and  $\Sigma_{\text{s},0}$  values; the introduction of interaction-driven SF would work in the direction of increasing both quantities.

As a consequence of the mentioned predictions, FA-R showed that the scatter around the stellar TFR due to  $\lambda$  ( $\Sigma_{\text{bar},0}$ ) should diminish compared to the one around the baryonic TFR; from the baryonic to the stellar TFR, the average scatter decreases from  $\sigma_{\text{intr}}(\text{Log}V_{\text{m}}) \approx 0.053$  to  $\sigma_{\text{intr}}(\text{Log}V_{\text{m}}) \approx 0.040$ . Galaxies that in the baryonic TFR were shifted to the high- $V_{\text{m}}$  side, because of their higher surface densities, transform gas into stars more efficiently and shift also to larger  $M_{\text{s}}$  values in the stellar TFR diagram compared to galaxies of lower surface densities. As a result, the dispersion in the stellar TFR due to disk surface density (mainly associated to  $\lambda$  and  $f_{\text{gal}}$ ) decreases, and *the TFR becomes almost the same for HSB and LSB galaxies: the anti-correlation between the residuals of the TFR and those of the  $R_{\text{s}}$ - $M_{\text{s}}$  relation disappears.* The dispersion in the halo MAH remains as the main source of scatter in the stellar TFR. However, regarding the original MAH dispersion, it is also predicted a kind of compensation in the shift of galaxies in the  $V_{\text{m}}$ - $M$  diagrams: galaxies that were shifted to the high- $V_{\text{m}}$  side because they were formed in halos assembled earlier (more concentrated), are also shifted to the larger- $M_{\text{s}}$  side because these galaxies had more time to consume their gas (they end up with higher  $f_{\text{s}}$ ).

The predictions of the  $\Lambda$ CDM-based disk galaxy mod-

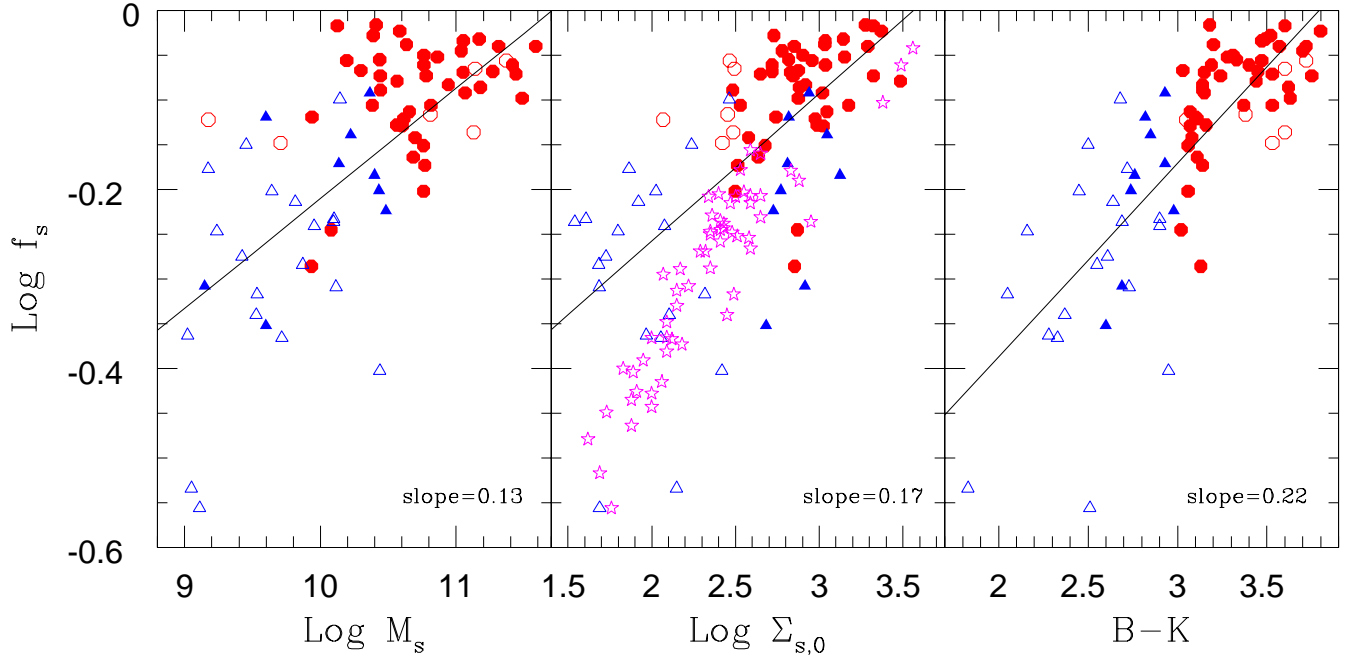


FIG. 7.— Stellar fraction  $f_s$  vs  $M_s$ ,  $\Sigma_{s,0}$ , and  $(B-K)$ . Solid and empty symbols are for HSB and LSB galaxies, respectively. Red galaxies are represented with circles, while blue galaxies with triangles. The solid lines are the Log-Log orthogonal linear regressions. Stars are from models by FA-R.

els provide an adequate context for interpreting the observational results plotted in the two upper rows of Fig. 6. The loss of dependence of the  $V_m$ - $M$  correlation residuals upon the  $R$ - $M$  correlation residuals when changing from baryonic to stellar quantities can be understood on the ground of the (self-regulated) SF efficiency dependence on disk surface density described above (see also Dutton et al. 2007). This also explains the reduction of the scatter around the TFR from the baryonic case to the stellar case (see Table 1), though the model results are more pronounced than observations both in the changes of the scatter values and in the slopes of the residual correlations.

In the same way, the distribution of galaxies in the diagrams of the residuals for the  $V_m$ - $M$ ,  $(B-K)$ - $M$ , and  $f_s$ - $M$  correlations (Fig. 6) can be interpreted as follows. Upon the understanding that disk color and  $f_s$  are related mainly to the halo MAH (concentration), the correlations between the baryonic residuals  $\Delta V_m(M_{\text{bar}})$  and  $\Delta(B-K)(M_{\text{bar}})$ , and between  $\Delta V_m(M_{\text{bar}})$  and  $\Delta f_s(M_{\text{bar}})$ , are expected (see above). This is because for a given mass, halos assembled earlier have larger  $V_m$ , and the galaxies formed inside them transformed gas into stars earlier (therefore are redder) and more efficiently (therefore have higher values of  $f_s$ ). In the corresponding panels of Fig. 6, one sees indeed these predicted tendencies, mainly for the HSB galaxies. For the LSB galaxies, the tendencies again (see §3.4) almost disappear. It might be because the (low) SF rate in LSB galaxies does not depend anymore on the gas infall rate; this dependence is what allowed us to associate the observables, color and  $f_s$ , to the halo MAH<sup>8</sup>. In the residuals

plots corresponding to stellar quantities, the tendencies become negligible because from  $M_{\text{bar}}$  to  $M_s$ , the shifts in  $V_m$  in the TFR, due to the halo MAH (concentration), tend to be compensated by shifts in  $M_s$  (see the previous paragraph). Therefore, *in the  $V_m$ - $M_s$  (stellar) diagram the mentioned SF effects tend to reduce the scatter and its dependence on surface density, color, and  $f_s$  compared to the  $V_m$ - $M_{\text{bar}}$  (baryonic) diagram.*

#### 4.3. The luminous relations

The slopes and scatters of the  $K$ -band scaling correlations are similar, within the uncertainties, to those of the stellar scaling correlations. The only quantity that actually changes in the diagrams is  $L_K$  for  $M_s$ , through the  $K$ -band mass-to-luminosity ratio,  $\Upsilon_K$ . This ratio increases slightly with the disk color for HSB galaxies and slightly decreases with it for blue LSB galaxies (§2.2). Hence, a significant trend of  $\Upsilon_K$  with mass or  $V_m$  is not expected. For the scale length, we assumed that  $R_s = R_K$ .

Interesting differences are seen between the  $K$ - and  $B$ -band scaling correlations. In the  $V_m$ - $L$  diagrams, the slope and intrinsic scatter increase significantly from the  $K$  to the  $B$  band. Calculating the ratio of the  $K$ - and  $B$ -band TFRs, we obtain:  $(B-K) \propto V_m^\delta$ , where  $\delta$  is  $-2.5$  times the difference of the  $B$ - and  $K$ -band slopes. This correlation is a consequence of the color- $L$  correlation shown already in Fig. 5. That the less luminous galaxies systematically tend to be slightly bluer, implies already a steepening of the slope when changing from the  $K$ - to the  $B$ -band TFR.

Furthermore, the residuals of the  $B$ -band TFR are correlated with those of the  $(B-K)$ - $L_B$  correlation, and less with the residuals of the  $R_B$ - $L_B$  and  $f_s$ - $L_B$  correlations: redder galaxies, with higher SB and  $f_s$  tend to be shifted to the TFR large- $V_m$  side; the opposite happens

makes the gas cooling very inefficient (Gerritsen & de Blok 1999).

<sup>8</sup> Below a certain gas surface density, the SF rate could be so inefficient that its long scale-time becomes independent of the gas infall rate (given by the MAH). Alternatively, the SF rate in LSB galaxies could be disconnected from the gas infall rate and the gas surface density as a consequence of their low metal content, which



for bluer galaxies, with lower SB and  $f_s$  (lowest row panels in Fig. 6). In fact, the step-wise backward analysis mentioned in §3.5 shows that the  $(B - K)$  color is a statistically significant parameter in the  $V_m$ - $L_B$ - $(B - K)$  multi-variable correlation, i.e. *color is the third parameter in the  $B$ -band TFR*, a result that other authors have also found in the optical bands (e.g., Verheijen & Sancisi 2001; Courteau et al. 2007; Kannappan et al. 2002, and more references therein). It is obvious that a galaxy in the  $V_m$ - $L_K$  diagram shifts to the large (low)  $B$ -band luminosity side if it is bluer (redder) than the corresponding average.

Why galaxies shifted to the high- (low-)  $V_m$  side in the  $B$  band TFR tend to be redder, with higher SBs and larger values of  $f_s$  (bluer, with lower SBs and smaller values of  $f_s$ )? According to the galaxy models discussed above, disks formed in halos with low  $\lambda$  and/or early mass assembling (high concentration), tend to consume gas into stars early in such a way that, for the same  $M_s$  or  $L_K$ , they result with older stellar populations (lower  $L_B$  and redder) and a higher  $f_s$  than those formed in halos with high  $\lambda$  and/or late mass assembling (low concentration). Thus, *while the dispersions introduced by  $\lambda$ ,  $f_{\text{gal}}$ , and the MAH are reduced by compensating effects in the stellar and  $K$ -band TFRs (§§4.2), the opposite happens in the  $B$ -band TFR*. We see indeed that the TFR in blue bands is systematically more scattered than in the near infrared bands (Table 1).

Regarding the  $R_B$ - $L_B$  correlation, its slope is significantly steeper than the one of the  $R_K$ - $L_K$  correlation. Again this is because, as the galaxy is more luminous, it tends to be redder, i.e., the  $L_B$ -to- $L_K$  ratio decreases with  $L$ . However, the situation is more complex than in the TFR case, because in the  $R$ - $L$  diagrams (i) the scatter is large and galaxies are strongly segregated by SB and color, and (ii) the  $B$ - and  $K$ -band radii are not the same as is the case of  $V_m$  in the TFR diagrams; the  $R_B$ -to- $R_K$  ratio tends to be larger for redder, more luminous galaxies. Thus, on one hand, the redder, higher SB galaxies shift to the low- $L$  and high- $R$  sides in the  $R$ - $L$  diagram when changing from band  $K$  to band  $B$ ; the shift tends to be larger for the more luminous galaxies (see Fig. 2). On the other hand, the bluer, lower SB galaxies shift slightly, mainly to the low- $L$  side, while the shift is larger for those of larger luminosities. As a consequence, the slope of the correlation increases in the  $B$  band and the scatter along the luminosity axis decreases.

In the  $V_m$ - $R$  diagrams, the correlations do not significantly change when changing from the  $K$  to the  $B$  bands. This confirms that the most relevant shifts in the  $R$ - $L$  diagrams are due to  $L$  rather than to  $R$ . The models predict that the scatter around the  $V_m$ - $R$  relation should thicken slightly in the band  $B$  with respect to the band  $K$ : galaxies of lower SBs and/or bluer (larger  $\lambda$ , late assembling halos, and lower  $f_{\text{gal}}$ ), which are shifted to the low- $V_m$  side in the  $K$  band, tend to shift also to larger  $B$ -band radii with respect to their  $R_K$  radii; for galaxies of higher SB and redder, the radii tend to be the same in both bands. According to Table 3, the direct intrinsic scatter around the  $V_m$ - $R_K$  and  $V_m$ - $R_B$  correlations is almost the same, while the inverse scatter (along the  $R$  axis), is larger in the  $B$  band.

#### 4.4. Quantitative comparisons

As shown, the predictions obtained with the  $\Lambda$ CDM-based models by FA-R offer an excellent qualitative description of several observational details of isolated disk galaxies. A systematic comparison of observations with results from models calculated with the most recent cosmological parameters will be presented elsewhere. With the aim to show that the models are able to provide even quantitative predictions, we plot those results from FA-R that can be compared with the observational inferences presented here. In FA-R, the authors plotted averages and scatters for three mass bins in the stellar TFR diagram (their Fig. 7), that we reproduce here in the corresponding panel of Fig. 1 (magenta stars with vertical error bars). We diminished their  $M_s$  points by the factor  $(0.70/0.65)^{-2}$  in order to take into account the slightly different value of  $H_0$  used in their models. The agreement is good, even more if we consider that models calculated with a  $\sigma_8 < 1$ , would have smaller values of  $V_m$ . The agreement is also quite good in the baryonic TFR diagram (magenta stars in the lower right panel of Fig. 1; the  $f_g$  values given in FA-R were used to calculate  $M_{\text{bar}}$  from  $M_s$ ). It should be stressed that models and observations are being now fairly compared; in both cases we have nearly isolated normal disk galaxies in a wide range of SBs and morphological types.

In FA-R were presented also model results for the  $R_s$ - $V_m$  relation, separated in HSB and LSB galaxies, but models with very high SB were not taken into account. We estimate the “weight” of these models in the fit for the HSB galaxies, and reproduce both the LSB and HSB+very HSB fits in the corresponding panel of Fig. 3 (thick magenta dashed lines), correcting the radii by a factor of  $(0.70/0.65)^{-1}$ . The agreement is rather good within the large scatter. Finally, model results by FA-R in the  $f_s$ - $\Sigma_{s,0}$  diagram (Fig. 7, magenta stars), and (ii) in the diagram of residuals of the baryonic  $V_m$ - $M_{\text{bar}}$  and  $R_{\text{bar}}$ - $M_{\text{bar}}$  correlations (upper left panel of Fig. 6, magenta dashed line) were presented already above, evidencing a reasonable agreement with observations; for the stellar case, the residuals do not correlate, as seen also for the observations.

### 5. POSSIBLE DIFFICULTIES FOR THE DISK $\Lambda$ CDM-BASED MODELS

The hierarchical  $\Lambda$ CDM-based models of disk galaxy evolution discussed above have been useful for interpreting the results reported in §3 about the slopes and scatters of the observed scaling relations in the different cases, as well as the behaviors of the residuals from these and other correlations. Even the zero-points of the relations predicted by FA-R seem to agree quantitatively with observations. Note that the models by FA-R, differentiate from others in the literature in that they *include a detailed description of disk SF and feedback and follow self-consistently the whole process of halo-disk evolution*. Although a detailed comparison with observations, using models calculated with more recent cosmological parameters, was left for a forthcoming paper, we may anticipate here some potential shortcomings of the model predictions as well as solutions.

(1) *The models are not able to explain the observed correlation of galaxy color with mass or luminosity*. In the hierarchical scenario, isolated more massive halos tend to assemble a given fraction of their present-day mass later

than the less massive ones. Then disks formed inside the more massive halos would tend to be younger (bluer) than those formed in the less massive halos. However, the models also show that the more massive is the halo, the higher is the surface density of the disk formed inside it (Dalcanton et al. 1997; FA-R); the higher the disk surface density, the more efficient the SF process and therefore, the redder the galaxy. As a result of these two evolutionary compensating effects, the models predict almost no dependence of color on  $M$  or  $L$  (e.g., Avila-Reese & Firmani 2000; Avila-Reese et al. 2005, see Table 5 therein). A possibility to produce a steeper color- $M$  correlation in the models is having a steeper disk surface density- $M$  dependence, which indeed is too shallow as compared with observations (see below). It should be said that the models do not include satellite galaxies and interacting-induced SF. For massive systems it is probable that the late gas infall is reduced by the large cooling time and because a fraction of the gas could have been trapped before into substructures that tend to be incorporated into the central galaxy through (minor) mergers; all these processes make the most luminous galaxies redder and with larger  $f_s$  values than obtained in the FA-R models.

An indirect dependence of galaxy color on  $L$  may appear also through environment. However, the disk galaxy sample studied in this paper includes field galaxies and galaxies from the UMA low-density, low mass cluster of galaxies. Therefore, it is less probable that environmental effects should produce the color- $L$  correlation. This correlation, which in some sense resembles the so-called *anti-hierarchical or downsizing galaxy formation* reported for early-type luminous galaxies (e.g., Cimatti, Daddi & Renzini 2006), could be produced by a mass (luminosity)-dependent dust extinction larger than the used here to correct the observations. Another alternative is related to the AGN feedback mechanism invoked recently to solve the sharp cut-off at the high-end of the (elliptical) galaxy luminosity function, as well as the observed downsizing of red early-type galaxies (e.g., Bower et al. 2006). Such a mechanism should be, however, strongly dependent on the galaxy mass in order to produce the observed continuous and monotone change of color with mass (luminosity) of disk galaxies.

(2) *The predicted dependence of surface density on mass (or SB on luminosity) is too shallow as compared to that inferred from observations*, although the latter is very noisy. Such a dependence can be estimated by combining the two simple model relations:

$$R_{\text{bar}} \propto \lambda g(c) R_h \propto \lambda g(c) (M_{\text{bar}}/f_{\text{gal}})^{1/3}, \quad (5)$$

$$R_{\text{bar}} \propto (M_{\text{bar}}/\Sigma_{\text{bar},0})^{1/2}.$$

By rejecting the small dependence of  $g(c)$  on mass (see Appendix C2), we then obtain that

$$\Sigma_{\text{bar},0} \propto M_{\text{bar}}^{1/3} f_{\text{gal}}^{2/3} / \lambda^2. \quad (6)$$

The semi-numerical evolutionary models show that the dependence of  $\Sigma_{\text{bar},0}$  on  $M_{\text{bar}}$  is even shallower than  $1/3$ . On the other hand, the slope (orthogonal regression) that we have found for the (noisy) correlation between  $\Sigma_{\text{bar},0}$  and  $M_{\text{bar}}$  in our galaxy sample is  $\sim 0.7$ , and it does not change significantly for the stellar and luminosity cases. Assuming that there is not a dependence

of  $f_{\text{gal}}$  and  $\lambda$  on mass, model predictions and observations would not agree: the surface density (brightness) of observed galaxies increases on average more rapidly with  $M$  ( $L$ ) than the models predict. Again, the inclusion of mergers and interaction-induced SF would work in the direction of increasing  $\Sigma_{\text{s},0}$  in the more massive galaxies.

On the other hand, recent inferences of the halo  $\lambda$  distribution for a large SDSS sub-sample of galaxies show this parameter to be systematically smaller and less scattered for more luminous galaxies (Cervantes-Sodi et al. 2007; Berta et al. 2008; see also Hernandez et al. 2007). By taking into account an anti-correlation of  $\lambda$  with mass in the models, both the color (1) and surface density (2) problems could be ameliorated without affecting significantly the scaling correlations. The question is why more massive galaxies would end with smaller values of  $\lambda$ —and consequently, higher surface densities—than the less massive ones. Cervantes-Sodi et al. (2007) suggested that the trend of  $\lambda$  with mass can be related to the halo angular momentum acquisition. A complementary explanation may lie in the baryon processes. For example, the outer gas in the most massive galaxy halos may not have enough time to cool and fall to the disk (for numerical results see e.g., van den Bosch 2002; Keres et al. 2005); the material located in the outer regions is the richest one in the specific angular momentum (Bullock et al. 2001b). On the other hand, in less massive halos the outer gas may flow through filaments to the disk, even before being shock-heated by the halo collapse (Keres et al. 2005). As a result, the specific angular momentum content will be higher in low mass galaxies and lower in the massive ones, which implies lower and higher disk surface densities, respectively. Note that this scenario implies also that more massive galaxies would tend to have lower values of  $f_{\text{gal}}$ . A mild anti-correlation of  $f_{\text{gal}}$  with mass in the models is allowed according to the observational results presented here (§§4.1): the  $V_{\text{m}}-R_{\text{bar}}$  relation would agree with the anti-correlation, while the  $R_{\text{bar}}-M_{\text{bar}}$  relation would do it in case  $\lambda$  also anti-correlates with mass, and regarding the  $V_{\text{m}}-M_{\text{bar}}$  relation, there is room for a mild variation of  $f_{\text{gal}}$  with mass. Detailed model calculations are necessary for obtaining more quantitative conclusions.

(3) *Are the scatters around the model and observed TFRs in agreement?* For the baryonic case, the agreement is marginal, being the scatter in the models slightly larger than in the observations (§§4.1). The difference could be even larger if (i) some of the simplifying assumptions introduced in the models are relaxed, which would increase the predicted scatter, and/or (ii) systematical errors like disk ellipticity are present, which would give rise to a reduction in our estimate of the observational intrinsic (physical) scatter<sup>9</sup>. Therefore, the current models of disk galaxy formation based on the  $\Lambda$ CDM cosmology have a potential problem in predicting the intrinsic scatter around the baryonic TFR. This scatter is smaller in the models for lower values of  $f_{\text{gal}}$  or for a distribution of  $\lambda$  narrower than the one of the  $\Lambda$ CDM halos. It could also be possible that the potential systematic errors, like disk ellipticity, confabulate with the disk surface density

<sup>9</sup> Some researchers have found evidence that disk ellipticity could account for roughly 50% of the observed scatter in the luminous TFR (Andersen et al. 2001; see also Franx & de Zeeuw 1992; Rix & Zaritsky 1995) or it could even explain all the observed scatter (Ryden 2004).



or baryonic-to-total mass ratio (with  $\lambda$  and  $f_{\text{gal}}$  from the models point of view) in such a way that the observed TFR scatter is diminished systematically.

For the stellar case, the scatter in the models becomes slightly smaller than in the observations (§4.2). Although in both cases (models and observations), the scatter decreases from the baryonic TFR to the stellar TFR, for models the decrease is more pronounced than for observations. However, there are known effects not considered in the FA-R models, like the interaction-induced SF, that will work certainly in the direction of increasing the scatter around the stellar TFR (e.g., Barton et al. 2007), but not around the baryonic one.

(4) *Are current models able to match both the TFR zero-point and the galaxy luminosity function?* First, we note that the disk galaxy evolutionary approach, like the one of FA-R, is different by construction to the semi-analytic models (SAM) or the halo occupation models (HOM): the former is focused on the modeling of the galaxy internal physics and evolution, while the latter are constructed for reproducing galaxy population global properties as the luminosity function. The parameters that the SAM and HOM need for reproducing in detail the observed luminosity function apparently produce a luminous TFR whose zero-point is shifted to the higher-velocity side with respect to observations (Baugh 2006, and references therein). Some astrophysical solutions were proposed to alleviate this apparent problem (e.g., Dutton et al. 2007; Gnedin et al. 2007).

However, before introducing modifications to the common disk galaxy formation scenario, we may mention at least four aspects that should be taken into account in order to compare fairly the predictions of SAM/HOM with observations in regards to the TFRs. (1) Since the TFRs are related to disk internal properties, a more detailed modelling of these properties than that carried out in the SAM is necessary; for example, in the SAM, disks are assumed to have a pure exponential mass distribution, the SF-feedback processes are artificially linked to the halo circular velocity, etc. (2)  $V_m$  is typically used to define the TFRs, while in the SAM/HOM only approximations to this velocity are calculated. (3) The TFRs refer only to the population of normal disk galaxies, while the luminosity function that the SAM/HOM fit to observations refers to the overall galaxy population. (4) The halos where disk galaxies form could be a subgroup of the overall halo population, for example those that did not suffer a major merger since  $z \sim 1$ ; therefore, the corresponding “disk galaxy” halo mass function, and not the overall one, should be used in the HOM as the starting point in the procedure of shaping the luminosity function.

From the point of view of the SAM and HOM, the passage from the halo mass function to the galaxy luminosity function implies a specific  $M_h$ -to- $L$  ratio as a function of mass. Recent studies using galaxy-galaxy weak lensing, allowed to determine directly the ‘central’ galaxy  $M_h$ -to- $L$  ratios (e.g., Hoekstra et al. 2005; Mandelbaum et al. 2006). For the FA-R models, which would agree very well with the baryonic and stellar TFRs if corrected for  $\sigma_8 < 1$ , we have available the  $B$ -band luminosities. The results from Mandelbaum et al. (2006) for *late-type* galaxies (notice that they differ from those of the early-type galaxies) are given in

the  $r$  band. By using  $\langle (B - R) \rangle = 1.2$  for late-type galaxies (de Jong 1996b) and  $(r - R) = 0.2$ , we estimate from the FA-R models  $\langle M_h/L_r \rangle / (M_\odot/L_{r,\odot}) = 62.2 \pm 9.1, 60.7 \pm 14.3$ , and  $77.6 \pm 26.5$ , for the luminosities  $\langle L_r \rangle / L_{r,\odot} = (5.6 \pm 1.1) \times 10^{10}, (5.7 \pm 1.2) \times 10^9$ , and  $(4.85 \pm 1.2) \times 10^8$ , respectively. To compare the FA-R  $M_h/L_r$  ratios with those of Mandelbaum et al., the values just reported should be increased by  $\approx 15\%$  due to the different definitions of  $M_h$ . The good agreement between models and observations within their scatters, is encouraging. We can also compare tracers of the inner luminous (or baryonic)-to-dark matter ratios of models and observed galaxies. For example, in ZAHF the disk-to-total velocity ratio at the maximum of the rotation curve was estimated for the same galaxies studied here. Models and observations were found to agree roughly, both in the zero-point as well as in the dependence of this ratio on the disk surface density or SB (see Fig. 3 in ZAHF).

Summarizing, the FA-R models based on the  $\Lambda$ CDM scenario seem to be able to predict both the TFR, including its zero-point, and the inferred, directly from observations,  $M_h$ -to-luminosity ratios of central late-type galaxies, as well as the inner luminous and baryonic-to-dark matter contents. These ratios, specially the former, are closely related to the “transfer” function needed for passing from the halo mass function to the galaxy luminosity function. We speculate that if the SAM and HOM take into account the shortcomings mentioned above, then the potential problem of fitting both the TFR zero-point and the luminosity function will be overcome. On the other hand, some of the initial condition parameters used in models like those of FA-R, could be modified accordingly, if any, to reproduce the disk galaxy luminosity function, while the TFRs (and the other scaling relations) would be yet in agreement with the observations. For example, the anti-correlation of  $f_{\text{gal}}$  with mass for luminous galaxies (motivated by the large cooling time in massive halos) that the SAM/HOM evoke could be allowed by the models as discussed in items 1 and 2 above.

## 6. SUMMARY AND CONCLUSIONS

A compiled sample of 76 normal (non-interacting) local disk galaxies of all morphological types and SBs has been used to construct and compare, among them, the luminous (bands  $B$  and  $K$ ), stellar and baryonic scaling relations. The required observational information for building up this sample implied detailed surface photometry in bands  $B$  and  $K$ , a dynamical determination of the rotation curve amplitude, and HI gas integrated flux data. We have corrected and processed the observational data homogeneously, and obtained several composite disk quantities and their uncertainties: global  $(B - K)$  colors, stellar masses and surface densities, gas (or stellar) fractions, and baryonic masses, surface densities and scale lengths. The objectives of this work were (i) to explore the changes of the disk galaxy scaling relations and their residuals as moving from optical to NIR bands, and to stellar and baryonic quantities, (ii) to look for interpretations of the results in the context of  $\Lambda$ CDM-based evolutionary disk galaxy models, and (iii) to show the necessity of larger samples similar to the one compiled here for constraining models of galaxy formation and evolu-

tion. A summary of the results is as follows:

- The slope of the baryonic TFR is shallower than the slopes of the stellar and  $K$ -band TFRs ( $\approx 0.31$  vs  $\approx 0.27$  and  $0.26$ ; orthogonal regression) and, in agreement with previous works, the slope of the  $B$ -band TFR is steeper than the one of the  $K$ -band TFR ( $\approx 0.32$  vs  $\approx 0.27$ ). The estimated average intrinsic scatters in  $\log V_m$  around the baryonic, stellar,  $K$ - and  $B$ -band TFRs are  $0.051$ ,  $0.045$ ,  $0.049$ , and  $0.063$  dex, respectively. Thus, the baryonic TFR is more scattered than the stellar TFR. A statistical analysis shows that the radius (or surface density) is a significant third parameter in the former relation, while the latter, as well as the  $K$ -band TFR, do not admit a third parameter. In the case of the  $B$ -band TFR, which is the most scattered, the  $(B - K)$  color is a significant third parameter.

- The  $R$ - $M$ ( $-L$ ) correlations are scattered and segregated strongly by disk SB and weakly by color. The slopes of the baryon, stellar, and  $K$ -band correlations are around  $0.30$  (orthogonal regression), while for the  $B$ -band relation, it increases to  $0.44$ . The scatter around the latter, projected in the luminosity axis, is smaller than that in the other correlations. The  $V_m - R$  correlations are the most scattered ones and are also segregated strongly by disk SB and less by color. The slopes have values of around  $0.5$ .

- The residuals of the baryonic  $V_m$ - $M_{\text{bar}}$  and  $R_{\text{bar}}$ - $M_{\text{bar}}$  correlations are anti-correlated, mainly for the HSB galaxies. The slope is  $-0.15 \pm 0.04$  (orthogonal regression), showing that the smaller the disk radius, for a given mass (higher surface density), the larger the disk contribution to  $V_m$ . For the stellar and  $K$ -band cases, the anti-correlation almost disappears. Thus, our results show that the correlations among the mentioned residuals are different for the baryonic, stellar,  $K$ - and  $B$ -band cases. While the correlation (or the lack of it) among the residuals in the baryonic case can be used to explore the dynamical importance of the halo/disk in galaxies, in the stellar and luminous cases the effects related to SF processes distort any pure dynamical interpretation of the results.

- In spite of the velocity-dependent internal extinction correction that we have applied, the  $(B - K)$  color correlates significantly with the logarithms of  $L_B$ ,  $L_K$ ,  $M_s$ , and  $M_{\text{bar}}$  (orthogonal regression slopes of  $0.61$ ,  $0.53$ ,  $0.56$ , and  $0.60$ , respectively). Noisy but steep correlations are observed between the surface densities and brightnesses and the corresponding masses and luminosities. The stellar fraction,  $f_s$ , correlates strongly with  $(B - K)$  and less with surface densities (brightnesses) and luminosities (masses). In all cases, the lowest SB galaxies break the latter correlations, suggesting a kind of threshold in the surface density, below which the SF rate is almost independent of it (and of  $M$  or  $L$ ) and of the gas infall rate.

We have discussed previous models of disk galaxy formation and evolution (including halo contraction, SF and disk feedback; e.g., FA-R) within hierarchically growing  $\Lambda$ CDM halos, under the assumption of gas-detailed angular momentum conservation. We showed the potentiality of these models to describe the observational inferences, as well as how such inferences can help us to constrain several of the model parameters. A crucial aspect in this endeavor is the correct comparison of models

with observations. The basic models refer to isolated normal disk galaxies. Therefore, the observational sample should be also for nearly isolated normal disk galaxies. We highlight the following conclusions:

- The slopes of the baryonic  $V_m$ - $M_{\text{bar}}$ ,  $R_{\text{bar}}$ - $M_{\text{bar}}$ , and  $V_m$ - $R_{\text{bar}}$  correlations can be interpreted as a direct imprint of the cosmological  $\Lambda$ CDM halo  $V_m$ - $M_h$ ,  $R_h$ - $M_h$ , and  $V_m$ - $R_h$  relations, especially the former (baryonic TFR), which is the tightest one. The models show that this relation is robust to systematical or statistical variations in the disk baryonic mass fraction,  $f_{\text{gal}}$ , for  $f_{\text{gal}} < 0.08$ . Then, the main sources of scatter are the dispersions in the halo spin parameter  $\lambda$  and halo MAH (or concentration). The FA-R models provide a lower limit to the scatter around the relation due to these two dispersions, namely  $\sigma_{\text{intr}}(\log V_m) \approx 0.053$  ( $f_{\text{gal}} = 0.05 = \text{const.}$ ), which is already slightly larger than our observational inference.

- In combination, the slopes and scatters of the baryonic  $V_m$ - $M_{\text{bar}}$ ,  $R_{\text{bar}}$ - $M_{\text{bar}}$ , and  $V_m$ - $R_{\text{bar}}$  correlations inferred here from observations, as well as the correlations among their residuals, imply that the average value of  $f_{\text{gal}}$  in normal disk galaxies could not be larger than  $\sim 0.05$  and that  $f_{\text{gal}}$  can not depend strongly on  $M$  (or  $L$ ); if any, a moderate anti-correlation with  $M$  is permitted. A trend of  $f_{\text{gal}}$  nearly independent on mass, with average values of  $f_{\text{gal}} < 0.05$ , have been reported recently by other authors, who extended the analysis to disk dwarf galaxies and inferred halo masses directly from the observational data (Blanton et al. 2007; see also Bradley et al. 2007; Begum, Chengalur & Karachentsev 2007).

- The models are able to explain qualitatively the observed (weak) anti-correlation among the residuals of the baryonic  $V_m$ - $M_{\text{bar}}$  and  $R_{\text{bar}}$ - $M_{\text{bar}}$  correlations and the related finding that radius (or surface density) is a third parameter in the former correlation. The physical parameter beyond these behaviors is  $\lambda$ . Model disks with low  $\lambda$  have high surface density and contribute significantly to  $V_m$ , in such a way that, for a given mass,  $V_m$  correlates with  $R_{\text{bar}}$  or  $\Sigma_{\text{bar},0}$ . Instead, disks with high  $\lambda$  values are of low surface density and have a negligible gravitational contribution to  $V_m$ ; then, the dependence of  $V_m$  on  $\Sigma_{\text{bar},0}$  (or on  $R_{\text{bar}}$  for a fixed mass) tends to disappear. The models can explain also why the anti-correlation among the residuals becomes negligible in the stellar or  $K$ -band cases: for a given mass, galaxies not only shift to the high- $V_m$  side in the TFR diagram as the radius is smaller ( $\Sigma_{\text{bar},0}$  is higher), but also shift to the high- $M_s$  (or  $L_K$ ) side due to a higher efficiency in transforming gas into stars. As a result, the scatter around the stellar TFR becomes independent of  $R_s$  or  $\Sigma_{s,0}$ , and smaller than in the baryonic case.

- The (self-regulated) SF efficiency effect just mentioned produces a dependence of the stellar mass fraction  $f_s$  on surface density (or brightness). Such a non-trivial prediction agrees roughly with the one found for our processed galaxy catalog (Fig. 7), and it is associated mainly with the  $\lambda$  parameter: the smaller the  $\lambda$ , the higher the disk surface density and the more efficient the transformation of gas into stars. Although less relevant,  $f_s$  and  $\Sigma_{s,0}$  are also affected by the gas infall history, which is connected to the cosmological halo MAH. Since the MAH plays a role in the scatter of the baryonic TFR, trends among the residuals of this rela-

tion and those of the color- $M_{\text{bar}}$  and  $f_s$ - $M_{\text{bar}}$  relations are predicted. These trends were found for our observational catalog, mainly for the HSB galaxies (Fig. 6). For LSB galaxies, it could be that the SF rate timescale becomes larger than the one of the gas infall rate, the connection between MAH and color/ $f_s$  then disappears.

• *Potential difficulties:* Our observational results show that both (i) the color- $M$  and (ii) surface density- $M$  correlations are steeper than the models would predict. We speculate that these shortcomings suggest that late minor mergers and interaction-induced SF, more common in massive galaxies, should play some role and/or that both, the galaxy spin parameter and  $f_{\text{gal}}$  anti-correlate with mass; at least qualitatively, both anti-correlations in combination are not expected to affect the scaling correlations presented here. (iii) The fact that the intrinsic scatter around the predicted baryonic TFR appears to be larger than the one inferred here, implies that there is no room for other physical or systematical sources of scatter around the TFR like disk ellipticity. On the other hand, the intrinsic scatter around the stellar TFR becomes smaller in the models than in the observations. However, external effects, as the interaction-driven SF, work in the direction of adding some scatter to the stellar TFR. (iv) The FA-R models (rescaled to  $\sigma_8 < 1$ ) agree with the observed baryonic and stellar TFR zero-points as well as with the  $M_h$ -to- $L$  ratios inferred directly from observations. The potential difficulty that the SAM/HOM find in matching both the TFR zero-point and the luminosity function could be solved by taking into account the shortcomings we have discussed in §5.

The results obtained in this work pose relevant questions for future studies. We showed that the determina-

tion of the scaling relations for disk galaxies in different bands and for stellar and baryonic quantities, as well as for the correlations among their residuals, bring valuable information on the nature and evolution of galaxies. The completion of large galaxy samples, unbiased and broad in properties, with detailed photometric, dynamic, and gas-content information is crucial for this kind of studies. The preferred approaches for such an undertaking are: follow-up observations in  $H_\alpha$  and/or HI emission lines for galaxies from the largest optical/NIR band surveys as SDSS (Pizagno et al. 2005), and synergy of existing wide-area homogeneous surveys conducted at optical/NIR bands and HI emission line, for example SDSS with HI surveys like ALFALFA (Giovanelli et al. 2005). According to the philosophy followed in this paper, the substantial advance comes from the adequate comparison of observations with theoretical models. Thus, in order to confirm, rule out, or perhaps expand, some of the conclusions attained here, a deep model exploration of the formation and evolution of the disk galaxy population should be carried out.

This work was supported by PAPIIT-UNAM grant IN107706 to V.A. and CONACyT grant 42810 to H.M.H. J. Z. acknowledges support from DGEP-UNAM and CONACyT scholarships, and support by the CAS Research Fellowship for International Young Researchers. J. Z. is supported by the Joint Program in Astrophysical Cosmology of the Max Planck Institute for Astrophysics and the Shanghai Astronomical Observatory. We are grateful to S. Courteau for comments to an early version of the manuscript and to the anonymous referee for his/her criticism and suggestions.

## APPENDIX

### A. ERROR BUDGET

In the following we describe how we estimate the uncertainties for the quantities we used to construct the scaling relations presented along the paper. We assume them to be Gaussian distributed, so our estimates refer to the standard deviation.

*B and K magnitudes:* we neglect the contributions to the errors due to uncertainties on the redshift, the extinction in our Galaxy, the disk thickness, and the  $k$  correction. Hence, the square of the error in the absolute magnitudes is estimated as the quadratic sum of the measurement error,  $\epsilon_m$  (given in the original papers used to compile the sample), and the one due to the correction for internal extinction,  $\epsilon_{A_i}$ :

$$\epsilon_{M_{abs}}^2 = \epsilon_m^2 + \epsilon_{A_i}^2, \quad (\text{A1})$$

To estimate  $\epsilon_{A_i}$  we take into account only errors related to the inclination of the galaxies,  $\epsilon_{b/a}$ , and neglect errors related to the empirical parameter  $\gamma$  (recall that  $A_i = \gamma(W_{20})\log(b/a)$ , Tully et al. 1998). Giovanelli et al. (1997) suggest to add also the error  $\epsilon_\gamma = 0.15\gamma$ , but this term is in most of the cases sub-dominant compared to the error in the inclination (see for instance fig. 2 of their paper); only for high inclination and high values of  $\gamma$  both terms may become comparable. Thus, we have:

$$\epsilon_{A_i} = \left(\frac{0.434}{b/a}\gamma\right)\epsilon_{b/a}, \quad (\text{A2})$$

where we assume  $\epsilon_{b/a} = 0.09 - 0.12(1 - b/a) + 0.037(1 - b/a)^2$ , following the estimation for the median error of  $\epsilon_{b/a}$  given by Giovanelli et al. (1997). Finally, the error in  $\log L$  is given by  $\epsilon_{\log L} = \epsilon_{M_{abs}}/2.5$ , where  $\epsilon_{M_{abs}}$  was given in equation (A1).

*Stellar mass:* the error in  $\log M_s$  is estimated as the quadratic sum of the logarithmic errors in  $L_K$  and in the mass-to-luminosity ratio  $\Upsilon_K$ :

$$\epsilon_{\log M_s}^2 = \epsilon_{\log L_K}^2 + \epsilon_{\log \Upsilon_K}^2, \quad (\text{A3})$$

where an uncertainty of 25% in the value  $\Upsilon_K$  was considered (Bell et al. 2003).

*Baryonic mass:* the error is calculated as the quadratic sum of the errors in  $M_s$  and  $M_g$ ,  $\epsilon_{M_{\text{bar}}}^2 = \epsilon_{M_s}^2 + \epsilon_{M_g}^2$ ; the corresponding logarithmic error in  $M_{\text{bar}}$  is then

$$\epsilon_{\log M_{\text{bar}}} = \frac{0.434}{M_{\text{bar}}} \epsilon_{M_{\text{bar}}} M_{\text{bar}}. \quad (\text{A4})$$

The error in  $M_g$  is calculated as:

$$\epsilon_{M_g} = M_g \frac{\epsilon_{S_\nu}}{S_\nu}, \quad (\text{A5})$$

where the measurement error  $\epsilon_{S_\nu}$  is taken as reported in the HyperLEDA information system.

*Scale lengths:* in order to estimate the fitting error in the scale lengths of the galaxies used here, we have experimented with the fit of the observed SB profiles by using both a marking-the-disk method and the bulge-to-disk decomposition method. We have seen that typical uncertainties in the determination of  $R$  by both methods are of the order of 5–10% (see also MacArthur et al. 2003; Graham 2002). There is a very weak systematical trend for larger lengths determined with the latter method relative to the ones determined with the former one from late to early morphological types. The uncertainty in  $R$  depends also on the SB profile type and other specific details. We finally decided to assign a logarithmic error of  $\epsilon_{\log R} = 0.05$  ( $\approx 11\%$ ) to the scale lengths in both the  $B$  and  $K$  bands, and  $\epsilon_{\log R} = 0.06$  for the baryonic case, where the gas disk also contributes to the final surface density profile.

*Rotational velocities:* the errors (standard deviations) in  $\log W_{20}$ ,  $\epsilon_{\log W_{20}}$ , were taken from the sources, namely Verheijen (1997), Verheijen & Sancisi (2001), and the HyperLeda information system.

## B. THE SCALING RELATIONS OF CDM HALOS AND DISK GALAXY FORMATION

Distinct CDM halos –those not contained within larger halos– can be characterized by the so-called virial mass and radius,  $M_{\text{vir}}$  and  $R_{\text{vir}}$ , and by a maximum circular velocity,  $V_{\text{m,h}}$ . Halos which are contained inside larger ones (sub-halos) have commonly radii and masses smaller than  $R_{\text{vir}}$  and  $M_{\text{vir}}$ , because their growth is truncated or even reversed due to tidal stripping;  $V_{\text{m,h}}$  is less affected by these effects. It is well known that the masses and maximum circular velocities of CDM halos, and even of sub-halos, correlate tightly as  $V_{\text{m,h}} \propto M_h^a$  with  $a \approx 0.32 - 0.30$ , where  $M_h$  is the virial or truncated mass of the halo (e.g., Navarro et al. 1997; Avila-Reese et al. 1998, 1999, 2005; Bullock et al. 2001a). The correlation is basically an imprint of the linear power spectrum of fluctuations, whose variance at the galaxy scales decreases very slowly (logarithmically) with the fluctuation mass. This rough scale invariance produces naturally the  $V_{\text{m,h}}-M_h$  relation for the collapsed CDM halos. The complex non-linear non-spherical hierarchical halo assembly process introduces only minor deviations upon this relation as well as a scatter. The cosmological TFR has an intrinsic scatter,  $\sigma_{\text{MAH}}(\text{Log} V_{\text{m,h}})$ , due mainly to the stochastic nature of the mass assembly histories, which produces also a scatter in the halo concentration parameter  $c$  (Avila-Reese et al. 1998, 1999; FA-R).

For distinct halos, by definition  $R_{\text{vir}} \propto M_{\text{vir}}^{1/3}$ ; sub-halos tend to follow a similar relation between  $R_h$  and  $M_h$ , but with some scatter and with a smaller proportionality coefficient. Consequently,  $V_{\text{m,h}}$  and  $R_h$  are also correlated, as  $V_{\text{m,h}} \propto R_h^\gamma$  with  $\gamma \approx 1 - 1.25$ , although extra scatter is introduced in this relation due to the variation in  $V_{\text{m,h}}$  for a given mass, as in the case of the  $V_{\text{m,h}}-M_h$  relation.

Disk galaxies are assumed to form inside the growing CDM halos from the trapped baryons. Therefore, the scaling relations of the halos are expected to be imprinted in the baryonic and stellar scaling relations of disk galaxies. Following, we describe the main physical ingredients of the FA-R models (see for details Avila-Reese et al. 1998; FA-R; Avila-Reese & Firmani 2000). An extended Press-Schechter approach is used to generate the MAHs of the halos from the primordial density fluctuation field, and a generalized secondary infall model is applied to calculate the time-by-time virialization of the accreting mass shells. The evolution and structure of the  $\Lambda$ CDM halos calculated in this way agree well with results from cosmological N-body simulations (Avila-Reese et al. 1999). The halo mass shells are assumed to have aligned rotation axis with specific angular momentum given by  $j_{sh}(t_v) = dJ(t_v)/dM_v(t_v)$ , where  $J = \lambda GM_v^{5/2}/|E|^{1/2}$ ,  $J$ ,  $M_v$  and  $E$  are the total angular momentum, mass and energy of the halo at the shell virialization time  $t_v$ . The halo spin parameter,  $\lambda_h$ , is assumed to be constant in time. As a result of the assembling of these mass shells, a present day halo ends with an angular momentum distribution close to the (universal) distribution measured by Bullock et al. (2001b) in N-body simulations.

A fraction  $f_{\text{gal}}$  of the mass of each shell is assumed to cool down and form a disk layer in a dynamical time. The radial mass distribution of the layer is calculated by equating its specific angular momentum to that of its final circular orbit in centrifugal equilibrium (detailed angular momentum conservation is assumed). The superposition of these layers form the disk, which tends to be steeper in the center and flatter at the periphery than the exponential law. The disk surface density distribution is mainly determined by the halo angular momentum distribution. For example, for a given halo of radius  $R_h$  and mass  $M_h$ , the characteristic size of the baryonic disk (and its typical surface density), described in a first approximation by the scale length,  $R_{\text{bar}}$ , is determined mainly by the halo spin parameter,  $\lambda_h$ . The distribution of  $\lambda_h$  found in analytical and numerical studies is well described by a log-normal function, whose median and dispersion almost do not depend on the halo mass. While here we assume that the pre- and post-disk formation spin parameters are equal,  $\lambda_h = \lambda_d$ , in most of our discussions, the quantity  $\lambda$  refers to the post-disk formation spin parameter and it could deviate from  $\lambda_h$  if the baryon angular momentum is redistributed (in the halo or inside the disk) or if not all the halo gas falls into the disk.

The gravitational interaction of disk and inner halo (important for estimating  $V_m$ ) is calculated using an extended adiabatic invariance formalism, which differs from the usual one in that we take into account the ellipticity of the orbits, i.e., the circular orbit assumption is relaxed. The disk SF at a given radius (azimuthal symmetry is assumed) is triggered by the Toomre gas gravitational instability criterion and self-regulated by a vertical disk balance between the energy input due to SNe and the turbulent energy dissipation in the ISM. This physical prescription yields naturally a Schmidt law with an index  $n \lesssim 2$ , slightly varying along the disk. The SF efficiency depends on the gas surface density determined mainly by  $\lambda$ , and on the gas accretion rate determined by the cosmological MAH. Finally, we estimate the mass of the (pseudo)bulge as the inner disk mass where the Toomre stellar parameter indicates disk instability.

### C. PREDICTIONS FOR THE BARYONIC SCALING RELATIONS

**(C1) The  $V_m$ - $M_{\text{bar}}$  relation.** In order to pass from the cosmological TFR to the baryonic one, we should pass (i) from the halo  $V_{m,h}$  to  $V_m$ , and (ii) from the halo mass  $M_h$  to  $M_{\text{bar}}$ . The latter is given simply by  $M_{\text{bar}} = f_{\text{gal}} M_h$ , where  $f_{\text{gal}}$  is the (central) galaxy mass fraction. The distribution of  $f_{\text{gal}}$  and its possible dependence on  $M_h$  and other halo properties is not well known. However, indirect and direct pieces of evidence show that  $f_{\text{gal}}$  should be much smaller than the universal baryon fraction,  $f_{\text{gal}} \ll \Omega_b/\Omega_{\text{dm}}$  (e.g., Mo et al. 1998; FA-R; Smith et al. 2001; Bell et al. 2003; Jiménez, Verde & Oh 2003; Pizagno et al. 2005; Hoekstra et al. 2005; Mandelbaum et al. 2006; Blanton, Geha & West 2007). Regarding item (i), the formation of the disk inside the dark halo and the gravitational drag produced on it, redistributes the inner mass profile. The  $V_m/V_{m,h}$  ratio increases with the disk surface density and the disk baryon fraction  $f_{\text{gal}}$ . For a given  $M_h$ , the disk has a larger surface density for a smaller value of  $\lambda$ . Therefore, the relation between  $V_{m,h}$  and  $V_m$  depends on both  $\lambda$  and  $f_{\text{gal}}$ :  $V_m/V_{m,h} = G(\lambda, f_{\text{gal}})$ . The function  $G(\lambda, f_{\text{gal}})$  has been approximated in Zavala (2003) from models of disk formation inside CDM halos based on Mo et al. (1998) and FA-R (notice that FA-R used an adiabatic contraction formalism generalized to elliptical orbits; as a result, the contraction is weaker than in the simpler case of circular orbits; see also Gnedin et al. 2004). If  $\lambda$  and  $f_{\text{gal}}$  do not depend on mass, then the function  $G$  is almost independent of mass, and then the baryonic TFR is expected to have a slope similar to the cosmological TFR. On the other hand, due to the gravitational disk-halo coupling, as  $f_{\text{gal}}$  decreases,  $G$  also decreases in such a way that the objects shift in the baryonic TFR diagram nearly parallel to the cosmological TFR. The function  $G$  becomes more sensitive to  $\lambda$  as  $f_{\text{gal}}$  becomes larger; for higher values of  $f_{\text{gal}}$ , a large variation in  $G$  is expected. This has deep implications for the scatter in the baryonic TFR.

The intrinsic scatter in the baryonic TFR has at least three sources: (i) the original scatter from the halo cosmological TFR, (ii) the scatter in  $V_m$  due to the dispersion in  $\lambda$ , and (iii) the scatter in both  $V_m$  and  $M_{\text{bar}}$  due to the average value and dispersion of  $f_{\text{gal}}$ . As mentioned above, the latter produces a shift of the models nearly along the same relation, in such a way that its effect on the baryonic TFR scatter is expected to be small for reasonable average values of  $f_{\text{gal}}$  ( $\lesssim 0.08$ ). The major contribution to the scatter comes from the dispersion in the spin parameter  $\lambda$ . For a given  $f_{\text{gal}}$  and  $V_{m,h}$ , different values of  $\lambda$  produce disks of different surface densities, and therefore different values of  $V_m$ ; such effect is accounted for by the function  $G$ . For a given distribution of  $\lambda$ , the scatter due to  $\lambda$ ,  $\sigma_\lambda$ , increases as  $f_{\text{gal}}$  increases. The scatter also increases slightly if we allow for a dispersion in  $f_{\text{gal}}$  around the mentioned values (Gnedin et al. 2007). The scatter in the halo  $V_{m,h}$ - $M_h$  relation,  $\sigma_{\text{MAH}}(\text{Log} V_{m,h})$ , arises because halos of a given mass that formed through a rapid mass assembling process are more concentrated and have a larger  $V_{m,h}$  than those assembled slowly (Avila-Reese et al. 1998, 1999). The magnitude of this scatter slightly decreases with mass and it has a value of  $\sigma_{\text{MAH}}(\text{Log} V_{m,h}) \approx 0.035$  for a  $\sim 10^{12} M_\odot h^{-1}$  halo according to cosmological numerical simulations (Avila-Reese et al. 1999, 2005). According to the FA-R models, the average scatter in the baryonic TFR is  $\sigma_{\text{intr}}(\text{Log} V_m) \approx 0.053$  ( $f_{\text{gal}} = 0.05 = \text{const.}$ ). This value is a lower limit under the assumptions made. It could be smaller if the distribution of  $\lambda$  is narrower than the one of the CDM halos. This could happen, for example, if disk galaxies form only in a subset of CDM halos biased to have  $\lambda$  distribution narrower than the overall sample (e.g., D’Onghia & Navarro 2007; Dutton et al. 2007; Gnedin et al. 2007), or if the baryon spin parameter becomes smaller due to angular momentum transport processes; then the galaxies formed from the low end of the halo  $\lambda$  distribution would not be disk type anymore.

**(C2) The  $R_{\text{bar}}$ - $M_{\text{bar}}$  relation.** According to the models of disk galaxy formation discussed above, for a given halo radius  $R_h$ , the typical size of the disk, for instance its scale length  $R_{\text{bar}}$ , is mainly proportional to  $\lambda g(c) R_h$ , where  $g(c)$  is a function that depends weakly on the NFW halo concentration parameter  $c$  (Mo et al. 1998), given on its own by the halo MAH. Recall that detailed angular momentum conservation was assumed. The weak anti-correlation of  $c$  with  $M_h$  introduces a very weak correlation in  $R_{\text{bar}}$  with  $M_{\text{bar}}$ . Therefore, if the model parameters  $\lambda$  and  $f_{\text{gal}}$  ( $\equiv M_{\text{bar}}/M_h$ ) do not depend on the mass, then the slope of the  $R_{\text{bar}}$ - $M_{\text{bar}}$  correlation is expected to be only slightly steeper than the slope of the  $R_h$ - $M_h$  correlation, which is  $\sim 0.33$  (Appendix B). However, the correlation is predicted to be highly scattered, with a systematical shift in the normalization due to  $\lambda$  (recall that  $R_{\text{bar}}$  is directly proportional to  $\lambda$  while  $M_{\text{bar}}$  in principle is independent of  $\lambda$ ), and also due to  $f_{\text{gal}}$  and  $c$ . The two first parameters determine the surface density of the disk, therefore in the  $R_{\text{bar}}$ - $M_{\text{bar}}$  diagram the scatter should be strongly correlated with the surface density, e.g.  $\Sigma_{\text{bar},0}$ . Notice that a dependence of  $\lambda$  or  $f_{\text{gal}}$  on mass would imply a change in the slope of the  $R_{\text{bar}}$ - $M_{\text{bar}}$  correlation. For example, if  $\lambda$  anti-correlates with mass, then this slope will be shallower than the one of the initial  $R_h$ - $M_h$  correlation, but if  $f_{\text{gal}}$  anti-correlates with mass, then the slope will be steeper.

**(C3) The  $V_m$ - $R_{\text{bar}}$  relation.** In the context of the simple models discussed along this Appendix, we have that  $V_m \propto G(\lambda, f_{\text{gal}}) V_{m,h}$  and  $R_{\text{bar}} \propto \lambda g(c) R_h$ . Thus, if for the  $\Lambda$ CDM halos  $V_{m,h} \propto R_h$ , then one obtains that  $V_m \propto [G(\lambda, f_{\text{gal}})/\lambda g(c)] R_{\text{bar}}$ . As mentioned above,  $g(c)$  correlates very weakly with mass, and hence with radius.

Then, if  $\lambda$  and  $f_{\text{gal}}$  are independent of mass, the expected  $V_{\text{m}}-R_{\text{bar}}$  correlation should be slightly shallower than the cosmological one. On the other hand, if  $f_{\text{gal}}$  correlates (anti-correlates) with mass, then the slope becomes steeper (shallower). The scatter around the  $V_{\text{m}}-R_{\text{bar}}$  correlation is expected to be the largest one of the three scaling relations. Galaxies are scattered in the  $V_{\text{m}}-R_{\text{bar}}$  diagram by their associated values of  $\lambda$ ,  $f_{\text{gal}}$  and  $c$ . Differences on each of these values spread the galaxies in a divergent way in both axis. Therefore, the scatter of the  $V_{\text{m}}-R_{\text{bar}}$  relation is expected to correlate significantly with both  $\Sigma_{\text{bar},0}$  and galaxy color. Recall that in the  $R_{\text{bar}}-M_{\text{bar}}$  diagram, galaxies are scattered by  $\lambda$  and  $c$  only along the  $R_{\text{bar}}$  axis. In the  $V_{\text{m}}-M_{\text{bar}}$  diagram the spread produced by these parameters is also only along one axis ( $V_{\text{m}}$ ), but furthermore, the spread produced by  $f_{\text{gal}}$  in both axes is in such a way that galaxies move nearly along the main relation; this is why the TFR is the less scattered among the three relations.

## REFERENCES

- Akritis, M. G., & Bershad, M. A. 1996, *ApJ*, 470, 706  
 Andersen, D. R., Bershad, M. A., Sparke, L. S., Gallagher, J. S., III, & Wilcots, E. M. 2001, *ApJ*, 551, L131  
 Avila-Reese, V. 2007, in “Stellar and Galactic connections between particle physics and astrophysics”, Eds. A Carramiñana et al., *Astroph. & Sp. Sc. Proceedings* (Springer), p. 115–164  
 Avila-Reese, V., Firmani, C. 2000, *RevMexAA*, 36, 23  
 Avila-Reese, V., Firmani, C., & Hernández, X. 1998, *ApJ*, 505, 37  
 Avila-Reese, V., Firmani, C. & Zavala, J., 2002, *ASP Conference Series*, v. 282, 137  
 Avila-Reese, V., Firmani, C., Klypin, A., Kravtsov, A. 1999, *MNRAS*, 309, 507  
 Avila-Reese, V., Colín, P., Gottlöber, S., Firmani, C., & Maultsby, C. 2005, *ApJ*, 634, 51  
 Barton, E. J., Arnold, J. A., Zentner, A. R., Bullock, J. S., & Wechsler, R. H. 2007, *ApJ*, 671, 1538  
 Baugh, C. M. 2006, *Reports of Progress in Physics*, 69, 3101  
 Begum, A., Chengalur, J. N., & Karachentsev, I. D. 2005, *A&A*, 433, L1  
 Bell, E. F., & de Jong, R. S. 2001, *ApJ*, 550, 212  
 Bell, E., Barnaby, D., Bower, R. G., de Jong, R. S., Harper, Jr, D. A., Hereld, M., Loewenstein, R. F. & Rauscher, B. J., 2000, *MNRAS*, 312, 470  
 Bell, E. F., McIntosh, D. H., Katz, N., & Weinberg, M. D. 2003, *ApJS*, 149, 289  
 Bell, E. et al. 2003, *ApJ*, 585, L117  
 Berta, Z., Jimenez, R., Heavens, A. F., & Panter, B. 2008, *ArXiv e-prints*, 802, arXiv:0802.1934  
 Blanton, M. R., Geha, M., & West, A. A. 2007, *ArXiv e-prints*, 707, arXiv:0707.3813  
 Bower, R. G., Benson, A. J., Malbon, R., Helly, J. C., Frenk, C. S., Baugh, C. M., Cole, S., & Lacey, C. G. 2006, *MNRAS*, 370, 645  
 Bruzual, A. G., 1983, *ApJ*, 273, 105  
 Bullock, J. S., Kolatt, T. S., Sigad, Y., Somerville, R. S., Kravtsov, A. V., Klypin, A. A., Primack, J. R., & Dekel, A. 2001a, *MNRAS*, 321, 559  
 Bullock, J. S., Dekel, A., Kolatt, T. S., Kravtsov, A. V., Klypin, A. A., Porciani, C., & Primack, J. R., 2001b, *ApJ*, 555, 240  
 Casertano, S., & van Gorkom, J. H. 1991, *AJ*, 101, 1231  
 Catinella, B., Haynes, M. P., & Giovanelli, R. 2007, *AJ*, 134, 334  
 Cervantes-Sodi, B., Hernandez, X., Park, Ch., & Kim, J. 2007, *ArXiv e-prints*, 712, arXiv:0712.0842  
 Cimatti, A., Daddi, E., & Renzini, A. 2006, *A&A*, 453, L29  
 Courteau, S., & Rix, H.-W. 1999, *ApJ*, 513, 561  
 Courteau, S., MacArthur, L. A., Dekel, A., van den Bosch, F., McIntosh, D. H., & Dale, D. 2003, arXiv:astro-ph/0310440  
 Courteau, S., Dutton, A. A., van den Bosch, F., MacArthur, L. A., Dekel, A., McIntosh, D. H., & Dale, D. A. 2007, *ApJ*, in press  
 Cowie, L. L., Songaila, A., Hu, E. M., & Cohen, J. G. 1996, *AJ*, 112, 839  
 Dalcanton, J. J., Spergel, D. N., & Summers, F. J. 1997, *ApJ*, 482, 659  
 de Blok, W. J. G., & Bosma, A. 2002, *A&A*, 385, 816  
 de Blok, W. J. G., van der Hulst, J. M. & Bothun, G. D., 1995, *MNRAS*, 274, 235  
 de Blok, W. J. G., McGaugh, S. S. & van der Hulst, J. M., 1996, *MNRAS*, 283, 18  
 de Jong, R. S. 1996a, *A&A*, 313, 45  
 de Jong, R. S. 1996b, *A&A*, 313, 377  
 de Jong, R. S. & van der Kruit, P. C., 1994, *A&ASS*, 106, 451  
 De Rijcke, S., Zeilinger, W. W., Hau, G. K. T., Prugniel, P., & Dejonghe, H. 2007, *ApJ*, 659, 1172  
 Dutton, A. A., van den Bosch, F. C., Courteau, S., & Dekel, A. 2005, *ArXiv Astrophysics e-prints*, arXiv:astro-ph/0501256  
 Dutton, A. A., van den Bosch, F. C., Dekel, A., & Courteau, S. 2007, *ApJ*, 654, 27  
 Eisenstein, D. J., & Loeb, A. 1996, *ApJ*, 459, 432  
 Firmani, C., & Avila-Reese, V. 2000, *MNRAS*, 315, 457 (FA-R)  
 Feigelson, E. D., & Babu, G. J. 1992, *ApJ*, 397, 55  
 Franx, M., & de Zeeuw, T. 1992, *ApJ*, 392, L47  
 Gerritsen, J. P. E., & de Blok, W. J. G. 1999, *A&A*, 342, 655  
 Giovanelli, R., et al. 2005, *AJ*, 130, 2598  
 Giovanelli, R., Haynes, M. P., Herter, T., Vogt, N. P., da Costa, L. N., Freudling, W., Salzer, J. J., & Wegner, G. 1997, *AJ*, 113, 53  
 Gnedin, O. Y., Kravtsov, A. V., Klypin, A. A., & Nagai, D. 2004, *ApJ*, 616, 16  
 Gnedin, O. Y., Weinberg, D. H., Pizagno, J., Prada, F., & Rix, H.-W. 2007, *ApJ*, 671, 1115  
 Graham, A. W. 2002, *MNRAS*, 334, 721  
 Gurovich, S., McGaugh, S. S., Freeman, K. C., Jerjen, H., Staveley-Smith, L., & De Blok, W. J. G. 2004, *Publ. of the Astr. Soc. of Australia*, 21, 412  
 Han, J., Deng, Z., Zou, Z., Wu, X.-B., & Jing, Y. 2001, *PASJ*, 53, 853  
 Hernandez, X., Park, C., Cervantes-Sodi, B., & Choi, Y.-Y. 2007, *MNRAS*, 375, 163  
 Hoekstra, H., Hsieh, B. C., Yee, H. K. C., Lin, H., & Gladders, M. D. 2005, *ApJ*, 635, 73  
 Isobe, T., Feigelson, E. D., Akritis, M. G., & Babu, G. J. 1990, *ApJ*, 364, 104  
 Jimenez, R., Verde, L., & Oh, S. P. 2003, *MNRAS*, 339, 243  
 Kannappan, S. J., Fabricant, D. G., & Franx, M. 2002, *AJ*, 123, 2358  
 Koda, J., Sofue, Y., & Wada, K. 2000, *ApJ*, 531, L17  
 Keres, D., Katz, N., Weinberg, D. H., & Davé, R. 2005, *MNRAS*, 363, 2  
 Kodaira, K. 1989, *ApJ*, 342, 122  
 McGaugh, S. S., de Blok, W. J. G. 1997, *ApJ*, 481, 689  
 McGaugh, S. S., Schombert, J. M., Bothun, G. D., & de Blok, W. J. G. 2000, *ApJ*, 533, L99  
 Mandelbaum, R., Seljak, U., Kauffmann, G., Hirata, C. M., & Brinkmann, J. 2006, *MNRAS*, 368, 715  
 Mayer, L., & Moore, B. 2004, *MNRAS*, 354, 477  
 Mo, H. J., Mao, S., White, S. D. M. 1998, *MNRAS*, 295, 319  
 Navarro, J. F., Frenk, C. S. & White, S. D. M. 1997, *ApJ*, 490, 493  
 Navarro, J. F., & Steinmetz, M. 2000, *ApJ*, 538, 477  
 Steinmetz, M., & Navarro, J. F. 1999, *ApJ*, 513, 555  
 Paturel, G. et al. 1997, *A&ASS*, 124, 109  
 Pizagno, J., et al. 2005, *ApJ*, 633, 844  
 Pizagno, J., et al. 2007, *AJ*, 134, 945  
 Rix, H.-W., & Zaritsky, D. 1995, *ApJ*, 447, 82  
 Ryden, B. S. 2004, *ApJ*, 601, 214  
 Schlegel, D. J., Finkbeiner, D. P., & Davis, M. 1998, *ApJ*, 500, 525  
 Shen, S., Mo, H. J., & Shu, C. 2002, *MNRAS*, 331, 259  
 Smith, D. R., Bernstein, G. M., Fischer, P., & Jarvis, M. 2001, *ApJ*, 551, 643  
 Tinsley, B. M., 1981, *MNRAS*, 194, 63  
 Tully, R. B., & Fisher, J. R. 1977, *A&A*, 54, 661  
 Tully, R. B. & Verheijen, M. A. W. 1997, *ApJ*, 484, 145  
 Tully, R. B., & Pierce, M. J. 2000, *ApJ*, 533, 744  
 Tully, R. B., Pierce, M. J., Huang, J., Saunders, W., Verheijen, M. A. W. & Witchalls, P. L., 1998, *AJ*, 115, 2264  
 van den Bosch, F. C., Abel, T., Croft, R. A. C., Hernquist, L., & White, S. D. M. 2002, *ApJ*, 576, 21  
 Verheijen, M. A. W. 1997, *PhD. Thesis*, Groningen University  
 Verheijen, M. A. W. 2001, *ApJ*, 563, 694  
 Verheijen, M. A. W. & Sancisi, R., 2001, *A&A*, 370, 765  
 Willick, J. A. 1999, *ApJ*, 516, 4  
 Willick, J. A., Courteau, S., Faber, S. M., Burstein, D., Dekel, A., & Strauss, M. A. 1997, *ApJS*, 109, 333  
 Yang, X., Mo, H. J., & van den Bosch, F. C. 2003, *MNRAS*, 339, 1057  
 Young, J. S. & Knezek, P. M., 1989, *ApJ*, 347L, 55  
 Zavala, J. 2003, *B.Sc. Thesis*, Universidad Nacional Autónoma de México  
 Zavala, J., Avila-Reese, V., Hernández-Toledo, H., & Firmani, C. 2003, *A&A*, 412, 633 (ZAHF)